



# Evaluation of the fatigue resistance of butt-welded joints in towers of wind turbines — a comparison of experimental studies with small scale and component tests as well as numerical based approaches with local concepts

R. Glienke<sup>1,2</sup> · F. Kalkowsky<sup>2</sup> · A. F. Hobbacher<sup>3</sup> · A. Holch<sup>2</sup> · M. Thiele<sup>4</sup> · F. Marten<sup>5</sup> · R. Kersten<sup>6</sup> · K.-M. Henkel<sup>7</sup>

Received: 31 August 2023 / Accepted: 5 November 2023  
© The Author(s) 2024

## Abstract

Wind turbines must endure a high number of load cycles during their service lifetime. Therefore, the fatigue strength verification plays an important role. Butt-welded joints are one of the most common structural details in the tower structure of wind turbines. In general, the nominal stress method is used for their fatigue verification. The Eurocode 3 part 1–9 is the current design standard for this field of application and defines the fatigue resistance by pre-defined FAT-classes. This paper presents recent results of fatigue tests on small-scaled specimens and large components with transverse butt welds to discuss the validity of the FAT-class. In addition, results from numerical simulations for the verification with the effective notch stress and the crack propagation approach are used for comparison. For this purpose, macroscopic measurements of the weld seam geometry and a 3D scan were used for a realistic consideration of the notch effect in the simulation. Based on the consistency between the numerical results and the fatigue tests, the influence of the seam geometry on the fatigue resistance was worked out. Furthermore, a prediction of the fatigue strength of butt-welded joints with plate thicknesses up to 80 mm was carried out.

**Keywords** Transverse butt weld · Weld imperfections · Wind turbine tower · Fatigue strength · Local approaches · Large components

---

Recommended for publication by Commission XIII - Fatigue of Welded Components and Structures

✉ R. Glienke  
ralf.glienke@hs-wismar.de

- <sup>1</sup> Department of Engineering, University of Applied Sciences in Wismar, Wismar, Germany
- <sup>2</sup> Fraunhofer Institute for Large Structures in Production Engineering IGP, Rostock, Germany
- <sup>3</sup> Department of Engineering, Jade University of Applied Sciences, Wilhelmshaven, Germany
- <sup>4</sup> Department of Engineering Structures, Federal Institute for Materials Research and Testing (BAM), Berlin, Germany
- <sup>5</sup> Department of Mechanical Engineering, Process Engineering and Maritime Technology, University of Applied Sciences in Flensburg, Flensburg, Germany
- <sup>6</sup> ENERCON GmbH, Aurich, Germany
- <sup>7</sup> Department of Mechanical and Naval Engineering, University of Rostock, Rostock, Germany

## 1 Introduction

“The development of a sustainable energy generation is one of the most significant tasks of our time” [1]. In Germany renewable energies shall provide about 60 % of the necessary electricity by 2035 and up to 80 % by 2050. As the electricity from on- and offshore wind farms provide a significant contribution for this goal, the capacity of wind turbines is rapidly increased with each new turbine generation. Common onshore wind turbines in 2022 had a capacity of almost 4.4 MW which corresponds to an increase of 10 % compared to the previous year. This increase is linked to a larger rotor diameter and a larger hub height [2]. For offshore wind turbines, a quite similar development can be observed. For the upcoming generation built in 2025, wind turbines with a capacity up to 15 MW are planned [2]. With increasing capacity, the requirements regarding wear, fatigue, and corrosion are becoming increasingly important. As the costs for the tower structure are about 20–30 % of the whole turbine,

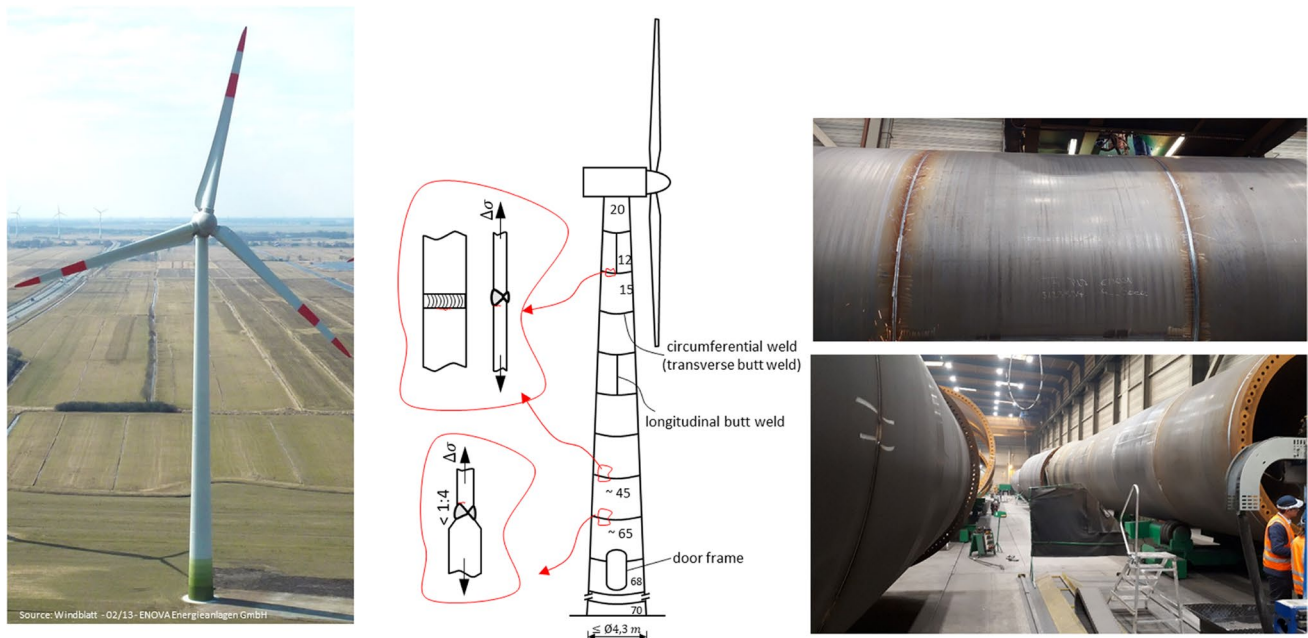
the optimization of the tower structure is a major issue in the wind energy business. In this context, the circumferential transverse butt-welded joints in the structure get into the focus (see Fig. 1).

In general, structural steel S355 is used for on- and off-shore steel tube towers. For onshore towers the plate thicknesses vary from 12 mm up to 70 mm, as offshore support structures for wind turbines currently have plate thicknesses up to 170 mm. Over the tower height, the plate thickness, and the diameter of the tower increase from top to bottom due to the increasing bending moment from the rotor thrust. However, at two locations, another specific increase to the plate thickness is needed, below the top flange (due to stiffness reasons) and around the door opening (due to buckling reasons).

The butt-welded joints are in full penetration with no systematic linear misalignment  $e$ . The standard welding process in manufacturing is the submerged arc welding process. Together with welding in flat position, high demands on manufacturing execution can be fulfilled which are necessary to achieve a required higher quality level acc. to the ISO 5817 [3]. A weld seam geometry with a reduced weld overfill  $h$  and smooth weld toe angles  $\alpha$  results in a lower notch effect and thus in a higher fatigue resistance [4]. Since FAT-classes for a transversely loaded butt weld categorised in guidelines and technical standards also cover weld seams with lesser welding quality, it is desirable to re-evaluate the FAT-class of butt-welded joints based on fatigue tests, especially for these high-quality weld seams.

In this context, the use of numerically based local approaches is a common way to investigate the influence of large plate thicknesses, because tests for such plates are very expensive. With the revision of the EN 1993-1-9 [5], the effective notch stress approach was added. In project ref. [6] for the re-evaluation and extension of the FAT-classes according to the Eurocode 3, it was noted that a large data base with  $n = 2,843$  fatigue test exists for butt-welded joints. However, complete documentation of the geometric dimensions of the welds is only available for a few tests. In addition, most of these tests were done with specimens, which had a plate thickness smaller than  $t = 25$  mm, as tests with plate thicknesses bigger than  $t = 40$  mm were not the subject of the belonging research studies. Within the range of the investigated plate thicknesses, no significant thickness reduction factor could be observed based on the results from fatigue tests. In contrast, numerical studies based on the effective notch stress approach in [6] show a clear dependence.

In this paper, an overview of the available guidelines and technical standards is given, which specify the fatigue resistance of butt-welded joints by a FAT-class for certain conditions and the main influencing parameters on the fatigue strength of butt-welded joints are briefly discussed. Then, results from new fatigue tests on butt-welded joints with and without different plate thicknesses up to a plate thickness of  $t = 40$  mm are presented. The new test results are flanked by additional large component tests shown for the first time. The results of the fatigue tests will be compared to results



**Fig. 1** Wind turbine from ENERCON at the wind farm Holtgaste (left), schematic illustration of essential welded structural details in steel towers (centre) and manufacturing of a tower section (right)

from the notch stress and the crack propagation approach for the tested specimens. In these analyses, the complete documentation of the weld seams geometry of the specimens is considered. All weld imperfections are measured by a macroscopic image. The results from this analysis show the potential of higher weld seam qualities when using submerged arc welding process regarding the fatigue resistance.

In a further step, the gained knowledge is used for an evaluation of different imperfections and their influence on the fatigue strength of butt-welded joints. For this purpose, the effective notch stress approach is applied on a real tower section, manufactured in accordance with quality level B of ISO 5817 [3]. This parameter study with typical weld seam imperfections from the submerged arc welding process is intended to show trends on the plate thickness influence. It will be shown that the limitation of the linear misalignment  $e = \min(0.1 \cdot t; 3 \text{ mm})$  according to quality level B has a favourable effect on the stress concentration and fatigue resistance for large plate thicknesses. The effect will also be discussed based on a 3D scan of a weld from a tower section. Finally, the fatigue strength will be evaluated both according to the specifications from technical standards and by numerical methods as the notch stress concept and fracture mechanics.

## 2 State of the art

### 2.1 Guidelines and technical standards for the evaluation of welded structural details

Table 1 contains a summary of the FAT-classes for butt-welded joints from guidelines and technical standards which use the nominal stress approach. In general, it can be assumed that the FAT-class 90 applies, which defines an allowable nominal stress range of  $\Delta\sigma = 90 \text{ N/mm}^2$  for  $N = 2 \cdot 10^6$  load cycles. One main difference between the different guidelines and technical standards is the definition of the thickness reduction factor. This factor is used for plate thickness greater than the reference thickness  $t_{\text{ref}} = 25 \text{ mm}$  and reduces the allowable stress range. Eurocode 3 [5, 7], the IIW-Recommendations [8], and the FKM-Guideline [9] use the formulation  $(t_{\text{ref}}/t)^{0.2}$  with the effective plate thickness  $t_{\text{eff}} = t$ . This equation is the result from experimental studies by Gurney [10]. Since the 7th edition of the FKM-Guideline, an additional thinness-effect for plate thickness equal or smaller than  $t = 25 \text{ mm}$  can be used. The thinness-effect increases the FAT-classes by a factor of 1.1 for plate thickness smaller than  $t = 10 \text{ mm}$ . Between a plate thickness of  $t = 10 \text{ mm}$  up to  $25 \text{ mm}$ , the positive influence is described by the equation  $f_t = (25 \text{ mm}/t)^{0.1}$ . In addition, a modified slope of  $m = 5$  for the S–N curve can be applied for plate thicknesses  $t < 7 \text{ mm}$ . The DNVGL-RP-C203 [11]

also uses the thickness reduction factor for plate thicknesses  $t > 25 \text{ mm}$  but with another definition for the effective plate thickness  $t_{\text{eff}}$ . The effective plate thickness  $t_{\text{eff}}$  is defined as the smallest value of  $t_{\text{eff}} = \min((16 \text{ mm} + 0.44 \cdot L_T); T)$  (see Table 1 for definition of  $L_T$  and  $T$ ). For butt-welded joints with large plate thicknesses and small weld bead width  $L_T$ , a higher fatigue resistance is caused by this equation compared to the Eurocode 3, IIW-Recommendations, or the FKM-Guideline. The problem of such an approach is that the structural engineer needs the information about the weld seam bead width from the manufacturing process already in the design phase. According to the BS 7608 [12], a thickness reduction factor must also be considered. In addition to this, a factor  $\Omega$  can be applied to the calculation. This factor considers global bending effects, which has a more favourable effect on fatigue. However, it is not applicable for secondary bending effects caused by a linear misalignment  $e$ . For butt-welded joints in crane steel structures, higher FAT-classes are generally applied. A thickness reduction factor is not included in EN 13001–3-1 [13]. The higher FAT-classes are due to the workshop production and better weld seam qualities.

### 2.2 Fatigue strength verification by nominal stresses

In general, the fatigue strength verification of structural details in towers of wind turbines is done with the global concept of the nominal stress approach. In this approach, the internal forces are used to determine the nominal stress at the failure location. These stresses are compared with the fatigue resistance, which is defined by FAT-classes with a S–N curve and a partial safety factor. The FAT-class is the result of extensive fatigue tests on specimens, which already contain the geometric notch effect (local stress concentration due to joint arrangement and weld seam geometry), the metallurgic notch effect, and the residual stresses. For components with high residual stresses, such as in the welded joints of towers for wind turbines, the nominal stress approach is independent from the mean stress.

### 2.3 Fatigue strength verification by the effective notch stress concept

Next to the fatigue strength verification with nominal stresses, alternative approaches with local concepts are increasingly used, e.g. due to the extension of the technical standards like prEN 1993–1-9 [5]. The effective notch stress concept as one of these local concepts is used, for example, when complex geometries do not allow the specification of a nominal stress [17]. Another reason may be the lack of structural details with a specific FAT-class. In comparison to the nominal stress approach, the effective

**Table 1** Comparison of the structural detail butt-welded joint from different guidelines and technical standards

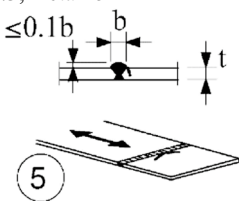
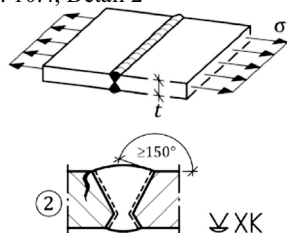
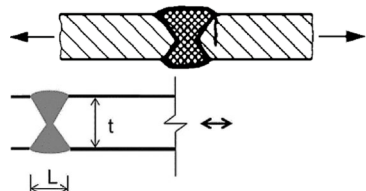
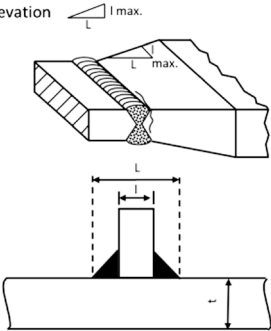
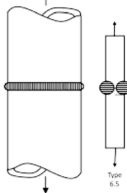
Steel structures			
Structural detail		Description	FAT
01	EN 1993-1-9:2010-12 [7] Tab. 8.3, Detail 5 	<b>Transverse splices in plates or flats</b> <u>Requirements:</u> - Welded from both sides - Weld run-on and run-off pieces to be used and subsequently removed, plate edges to be ground flush in direction of stress. - checked by NDT - Height of weld convexity $h \leq 10\%$ of weld bead width $b$ <u>Thickness reduction factor:</u> for $t > 25$ mm: $k_s = (25 \text{ mm}/t)^{0.2}$	90
02	prEN 1993-1-9:2023 (E) [5] Tab. 10.4, Detail 2 	<b>Splices in plates or flats of same thickness</b> <u>Requirements:</u> - Welded from both sides in welding position PA (acc. to DIN EN ISO 6947 [14]) - Weld ground flush at plate edges in direction of stress, where relevant, after removing weld run-off pieces. - As welded with flank angle $\alpha \geq 150^\circ$ - Linear misalignment $e \leq 5\%$ of plate thickness $t$ - An eccentricity is considered by appropriate nominal stress modification. <u>Thickness reduction factor:</u> for $t > 25$ mm: $k_s = (25 \text{ mm}/t)^{0.2}$	90
03	IIW-Recommendations 2016 [8] Table 3.1, No. 212 	<b>Transverse butt weld</b> <u>Requirements:</u> - Welded from both sides, weld made in shop in flat position - Weld run-on and run-off pieces to be used and subsequently removed, plate edges to be ground flush in direction of stress. - Misalignment 5 % of plate thickness $t$ - Weld reinforcement 10 % of thickness $t$ - NDT  <u>Thickness reduction factor:</u> for $t > 25$ mm: $f(t) = (t_{\text{ref}}/t_{\text{eff}})^{0.2}$ with $t_{\text{ref}} = 25$ mm for $L/t > 2$ : $t_{\text{eff}} = t$ for $L/t \leq 2$ : $t_{\text{eff}} = \max(0.5 \cdot L; t)$	90

Table 1 (Continued)

**Steel structures**

Structural detail	Description	FAT
<p>04 <b>BS 7608:2014 [12]</b> Table 5, No. 5.2</p> 	<p><b>Transverse butt weld</b> <u>Requirements:</u></p> <ul style="list-style-type: none"> <li>- Made from both sides by any arc welding processes in any position.</li> <li>- Proved free of all flaws which are likely to degrade the joint below its stated classification (see BS 7608:2014, 14.3.4).</li> <li>- These classifications do not include allowance for any misalignment of the joint.</li> </ul> <p><u>Thickness reduction factor by consideration of global bending stress:</u></p> <p>for <math>t &gt; 25</math> mm: <math>k_{tb} = (25 \text{ mm}/t_{\text{eff}})^{0.2} \cdot [1 + 0.18 \cdot \Omega^{1.4}]</math></p> <p>for <math>4 \text{ mm} \leq t \leq 25</math> mm: <math>k_{tb} = \{1 + \Omega[(25 \text{ mm}/t)^{0.2} - 1]\} \cdot [1 + 0.18 \cdot \Omega^{1.4}]</math></p> <p><u>Without global bending stress: <math>\Omega = 0</math></u></p> <p>for <math>t &gt; 25</math> mm: <math>k_{tb} = (25 \text{ mm}/t_{\text{eff}})^{0.2}</math></p> <p>with <math>L/t &gt; 2</math>: <math>t_{\text{eff}} = \max(25 \text{ mm}; t)</math></p> <p>and <math>L/t \leq 2</math>: <math>t_{\text{eff}} = \max(25 \text{ mm}; 0.5 \cdot L)</math></p> <p>for <math>4 \text{ mm} \leq t \leq 25</math> mm: <math>k_{tb} = 1</math></p>	D (90)
<p>05 <b>BS 7608:2014 [12]</b> Table 5, No. 6.5</p> 	<p><b>Steel pipes or tubes</b> <u>Requirements:</u></p> <ul style="list-style-type: none"> <li>- Weld made from one or both sides</li> <li>- Proved free of all flaws which are likely to degrade the joint below its stated classification (see BS 7608:2014, 14.3.4).</li> <li>- This classification does not include allowance for any misalignment of the joint or a thickness change.</li> </ul> <p><u>Thickness reduction factor:</u> see BS 7608:2014, Table 5, No. 5.2</p>	D (90)

**Mechanical engineering**


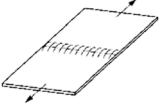
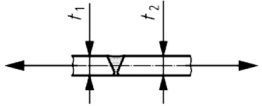


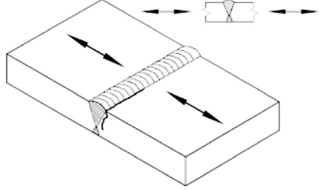
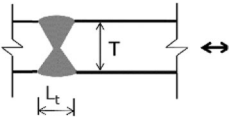
Structural detail	Description	FAT
<p>06 <b>FKM-Guideline 2020 [9]</b> Table 5.4.1, Detail 212 ([IIW])</p> 	<p><b>Transversely loaded butt weld</b> <u>Requirements:</u></p> <ul style="list-style-type: none"> <li>- Made in shop in flat position</li> <li>- Height of weld convexity <math>h &lt; 10</math> % of plate thickness <math>t</math></li> <li>- Misalignment <math>e \leq 5</math> % of plate thickness <math>t</math></li> <li>- NDT</li> </ul> <p><u>Thickness reduction factor:</u></p> <p>for <math>t \leq 10</math> mm: <math>f_t = 1.1</math></p> <p>for <math>10 \text{ mm} &lt; t \leq 25</math> mm: <math>f_t = (25 \text{ mm}/t)^{0.1}</math></p> <p>for <math>t &gt; 25</math> mm: <math>f_t = (25 \text{ mm}/t)^{0.2}</math></p>	90

Table 1 (Continued)

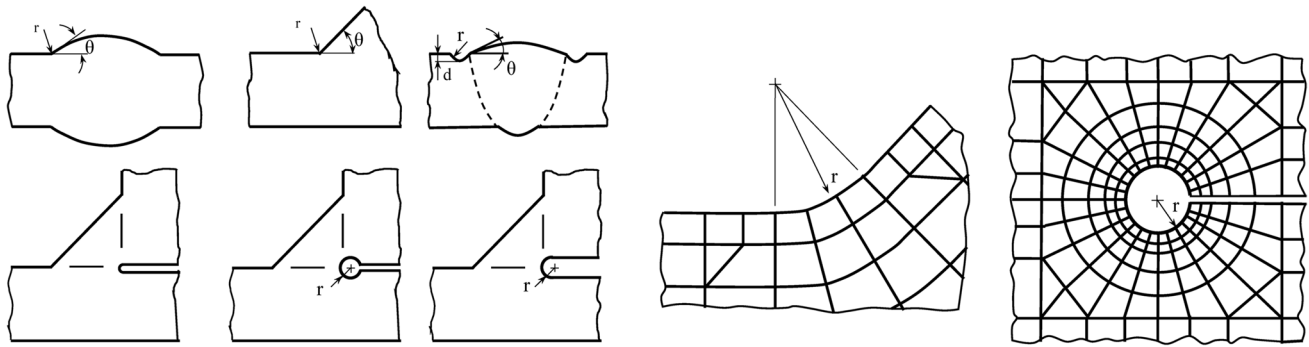
<b>Crane steel structures</b>			
<b>Structural detail</b>	<b>Description</b>		<b>FAT</b>
07 EN 13001-3-1:2019-03 [13] Table D.3, Nr. 3.1	 <b>Symmetrical butt weld, normal stress transverse to weld</b> <b>Requirements:</b> - Symmetrical plate arrangement - Welded through seam - Angular misalignment $\beta < 1^\circ$ - Quality level B		
	<b>Components with normal residual stresses</b> $t_1 = t_2$ or slope $\leq 1:3$		125
	<b>Components with high residual stresses</b> $t_1 = t_2$ or slope $\leq 1:3$		112
	<b>Components with high residual stresses</b> slope $\leq 1:2$		100
<b>Support structures for wind turbines</b>			
<b>Structural detail</b>	<b>Description</b>		<b>FAT</b>
08 DNVGL-RP-C203:2019-09 [11] Table A.5, No. 4	 <b>Transverse splices in plates and flats</b> <b>Requirements:</b> - Made in flat position in shop. - Weld run-on and run-off pieces to be used and subsequently removed, plate edges to be ground flush in direction of stress. - Height of weld convexity $h \leq 10\%$ of weld bead width $b$ - misalignment $e \leq 10\%$ of thickness $t$ for plates - misalignment $e \leq 5\%$ of thickness $t$ for tubes		D (90)
	<b>Thickness reduction factor:</b> for $t > 25$ mm: $(t_{\text{eff}}/25 \text{ mm})^{0.2}$		
	with: $t_{\text{eff}} = \min((14 \text{ mm} + 0.66 \cdot L_t); T)$		
09 IEC 61400-6:2020-04 [15]	Reference to EN 1993-1-9:2005, Tab. 8.1 to 8.10 and B.1 and EN 1993-3-2:2006, Annex C		
10 DIN 18088-3:2019-01 [16]	Reference to DIN EN 1993-1-9:2010-12, Tab. 8.1 to 8.10 and B.1		

notch stress approach considers the stress concentration at the point of failure caused by the weld seam geometry for the assessment. The effective notch stress can be determined by numerical simulation. As the plate thickness effect is already taken into account by the modelling of the FE model, no further reduction factor needs to be considered in this approach. The IIW-Recommendations [8] and the DVS-Technical Code 0905 [18] contain practical recommendations to determine the effective notch stress by numerical simulations. The failure location of the weld seams must be rounded with a fictitious radius (see Fig. 2). This size of the fictitious radius depends on the plate thickness in the analysis.

In this paper, results from fatigue tests on butt welds with plate thicknesses greater than  $t > 5$  mm are presented. For this structural detail, the weld toe is the failure location, so it was rounded according to the effective notch stress concept.

The fictitious radius is based on the consideration of the micro-supporting effect acc. to Neuber [19] in the interpretation for welded joints by Radaj [20]. The micro-supporting effect is gathered via the stress averaging approach. This approach has been successfully used to evaluate the fatigue strength of welded joints made of normal strength steel and plate thickness range  $1 \text{ mm} < t < 20 \text{ mm}$  [18]. The fatigue resistance acc. to the effective notch stress concept is defined





**Fig. 2** Recommendation according to IIW-Recommendations [8] for the rounding of the weld toe and root of different notch details (left), execution of the notch radius meshing (right)

as FAT 225 for  $N = 2 \cdot 10^6$  number of cycles for welded steel joints. This resistance value is the result of extensive experimental fatigue tests on different welded structural details. For smaller plate thicknesses, failure at the weld root or welded joints made of aluminium, different resistances exist. For the determination of the notch stress  $\sigma_e$  from numerical simulations with linear-elastic material behaviour the maximum principal stress at the failure location is used. This value is verified against the FAT 225. A verification with Mises-equivalent stresses against FAT 200 acc. to prEN 1993-1-9 [5] is also possible. The stress concentration factor  $K_t$  can be determined acc. to Equation (1), if the effective notch stress  $\sigma_e$  and the nominal stress  $\sigma_n$  are known:

$$K_t = \frac{\sigma_e}{\sigma_n} \tag{1}$$

The resistance nominal stress  $FAT_n$ -value from the notch stress calculation is FAT 225 divided by the stress concentration factor  $K_t$ , as shown in (2):

$$FAT_n = \frac{FAT_{225}}{K_t} \tag{2}$$

Further approaches for evaluating the fatigue strength of welded joints are described in the technical standards. A summary and evaluation of the different approaches used in [8] can be found in [21–23]. In the following, the crack propagation concept will be explained in more detail.

### 2.4 Fatigue strength verification based on fracture mechanics

Cyclic loaded structures are prone to fatigue failure. Here, the whole fatigue life of a structure can be subdivided into the three phases crack initiation, crack propagation, and failure of the residual cross-section. In welded joints without post treatment, the proportion of crack initiation in the entire fatigue life is small and thus can be neglected. This neglect

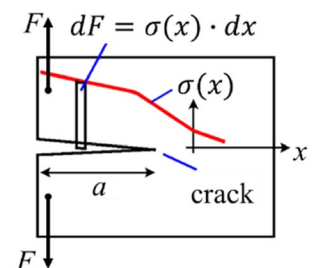
is on the conservative side. The phase, where the crack propagation is driven by elastic–plastic material mechanisms (short crack behaviour) can be covered by the choice of a damage equivalent initial crack  $a_0$ . The crack propagation calculation is performed by the use of the PARIS-ERDOGAN law from Eq. (3), starting with the initial crack  $a_0$  to a final one, which usually has a crack length of half of the plate thickness  $t$ .

$$\frac{da}{dN} = C_0 \cdot \Delta K^m \text{ for } \Delta K \geq K_{th} \text{ else } \frac{da}{dN} = 0 \tag{3}$$

$C_0$  and  $m$  are material constants. The stress intensity factors  $K = \sigma \sqrt{\pi a} \cdot Y(a)$  can be determined by parametric correction formulae  $Y(a)$ , which may be found in the relevant literature for usual joint configurations e. g. in BS 7910:2019 [24], API 579-1/ASME FFS-1 [25], or in FKM-Guideline for Fracture Mechanics Verification [26]. In many cases, these formulae cannot cover special geometries such as e. g. all types of misalignments. In those cases, the application of the weight function approach is recommended.

The idea of a weight function is that a force and the resulting stress intensity factor at the crack tip are considered (see Fig. 3). This is done for different distances  $x$  and different crack lengths  $a$ . The results may be presented in form of a table or an interpolation formula  $h(x, a)$ . Now, an arbitrary stress distribution can be described as a sum of the differential forces  $dF$ . The stress intensity factor  $K$  is received by a simple integration. The integration procedure

**Fig. 3** Weight function as summation of the differential forces  $dF$



must be programmed only once. It can be used for all types of stress distribution. Here, the weight function formula by NIU and GLINKA has been used. The advantage of the method is that only a stress distribution must be determined by FEA, which reduces the computational effort considerably.

$$dF = \sigma(x) \cdot dx \quad (4)$$

$$dK = dF \cdot h(x, a) \quad (5)$$

And so

$$K = \int_{x=0}^{x=a} \sigma(x) \cdot h(x, a) \cdot dx \quad (6)$$

If a crack grows larger and the stress intensity factor approaches the fracture toughness of the material  $K_{mat}$ , then the crack propagation accelerates. This effect can be covered by Eq. (7).  $K_{mat}$  can be estimated from Charpy-V-notch test data and the SANZ correlation [27].

$$\frac{da}{dN} = \frac{C_0 \cdot \Delta K^m}{(1 - R) \cdot \frac{maxK}{K_{mat}}} \quad (7)$$

For the material constant  $C_0$ , there is to distinguish between a wrought and a cast material (Table 2). The first is for cracks in the base material, e. g. at weld toes, and the second for root cracks through the weld deposit material. The constant  $m$  shall be assumed as  $m = 3.0$ .

At this point, different definition of a crack depth must be considered. The definitions may be contradictory:

- Technological crack of approx.  $a = 1$  mm, a conventional value often used
- Smallest detectable crack depth  $a = 2$  mm acc. to BS 7910:2019 [24]
- Crack depth by EN 1993–1-10 [28] of  $a = 0.5 \cdot \ln(t)$ , giving  $a = 1.5$  mm at  $t = 20$  mm plate thickness
- Requirement of free of cracks (?) acc. to ISO 5817:2023–07 [3]
- Equivalent initial crack for “crack free“ welded joints of  $a = 0.1 \dots 0.15$  mm

The requirement “crack free“ according to ISO 5817 [3] can hardly be verified by the existing NDT methods. Therefore, it must be relied on experience and confidence instead.

NDT may serve to give an indication, if the confidence in production is still justified. An adequate safety must be assured by regular inspection or redundancy of the structure.

## 2.5 Parameters influencing the fatigue strength of butt-welded joints

The different influencing parameters on the fatigue strength of welded joints cannot be considered isolated from each other as there is often an interaction between these parameters. The parameters described in the following are the most important ones for butt-welded joints (however, there is no claim to completeness). The fatigue behaviour of welded joints in condition “as welded” is characterised by a short crack initiation phase related to the total service life. Due to this behaviour, the fatigue strength of welded joints is more or less independent of the material strength. Welded joints behave like components with high notch effects or corroded components. Therefore, the FAT-class depends only on the material group and not on its strength. Surface conditions as the waviness from steel machining, slight corrosion, minor near-surface damages to the rolling skin, or roll inclusions only have a minor influence on the fatigue resistance of welded components. In contrast the weld toe or root dominates the fatigue resistance due to the high(er) notch effect. Small-scaled specimens (except longitudinal stiffeners) generally show a mean stress influence regarding the fatigue resistance. Welded assemblies, on the other hand, behave differently. For specimens like structural components, the influence of mean stress is relatively small. This is due to high residual stresses. They are usually in the region of the yield strength of the base material at the critical crack location. In welded structures with high residual stresses like tower segments of wind turbines, residual stresses and load stresses superpose. As a result, the effective stress at the weld toe is always a tensile stress, which leads to an independency from the present mean stress level. That is why small-scaled specimens need to be tested with high tensile mean stresses or  $R$ -ratios. The geometric shape of a welded joint (cruciform joints, butt joints, etc.) is the most important parameter regarding its fatigue resistance. In addition, the weld seam geometry at the weld toe or root has a big

**Table 2** Overview material parameter  $C_0$  as a function of crack location

Crack location	Material parameter $C_0$ [N;mm]	
Characteristic value of base material	$3.00 \cdot 10^{-13}$	API / ASME [25]
Characteristic value of weld deposit material	$5.21 \cdot 10^{-13}$	BS 7910 [24]
Mean value used in EN 1993–1-10	$1.80 \cdot 10^{-13}$	GURNEY TWI [10]



influence. A third important effect is metallurgical notches or seam defects by porosity and slag inclusions.

Figure 4 shows different failure modes of butt-welded joints. In general, butt-welded joints fail at the weld toe (Fig. 4a). For butt welds with flat seams and smooth seam transitions, the crack location can occur also between cover seam layers as shown in Fig. 4c. For butt-welded joints of different plate thickness and no linear misalignment  $e$ , the failure may occur on site with larger nominal cross-section (see Fig. 4d). Figure 4b also shows a failure starting from an inclusion. For this failure mode the crack propagation path runs from the in- to the outside. In service condition, this cannot be detected by regular inspections using near-surface non-destructive testing technique [4, 29].

Further effects are caused by the component dimension. For components with larger plate thicknesses and a comparable weld geometry, a higher notch effect at the weld toe results, especially due to greater residual stresses. During crack propagation, the crack initially localises in a larger area of unfavourable tensile stress, which leads to a higher crack propagation rate according to [30]. With increasing weld volume also, the possibility of irregularities increases. This is justified with the statistical influence of size.

## 2.6 Limits of imperfect shape and dimension acc. to ISO 5817

The fatigue resistance of butt-welded joints is significantly influenced by local imperfections. Table 3 contains the permissible limits for different imperfections of butt welds according to quality level B of ISO 5817 [3]. According to DIN 18008-3 [16], the execution class EXC3 is required for the shell of a steel tube tower. In conformity with paragraph 7.6.1 of EN 1090-2 [31], the limits for the imperfections of quality level B acc. to ISO 5817 [3] must be complied. Higher quality requirements are specified by the quality level

B125, which are described in the Annex C of the ISO 5817 [3]. The quality level B125 defines the requirements to achieve a fatigue resistance of FAT 125. It should be noted that the fulfilment of the requirements is not achieved by welding alone. In addition, the authors would like to emphasise that the tower sections do not have an angular misalignment  $\beta$  in the execution practise.

## 3 Experimental studies

### 3.1 Specification for performing fatigue tests on welded joints

There is no generally applicable standard for determining the fatigue strength of welded joints. Nevertheless, the most important specifications according to the IIW-Recommendations [8], the ISO/TR 14345 [32], DVS-Technical Code 2403 [33], and the Eurocode 3 part 1-9 [7] and its revision [5] should be mentioned with regard to the test programme. The IIW-Recommendations [8] requires testing at a high tensile mean stress level with a load ratio of  $R = 0.5$ . For tests done at lower tensile mean stress level, experimental FAT-values need to be reduced by 20 %. According to the authors, this assumption is not generally to be applied. Especially for welded joints with post weld-treatment and small notch effects, this requirement is not purposeful. The ISO/TR 14345 [32] defines for the tests on small-scaled specimen a high mean stress level or a high load ratio  $R$ . The nominal stresses must be below the yield strength of the base material. By this requirement, the high residual stress in the real structure shall be covered in the fatigue tests with small-scaled specimen. This leads to S-N curves that have a steeper slope and are below those with low mean stresses. According to Eurocode 3 part 1-9 [7], Sect. 7.1, at least  $n = 10$  tests

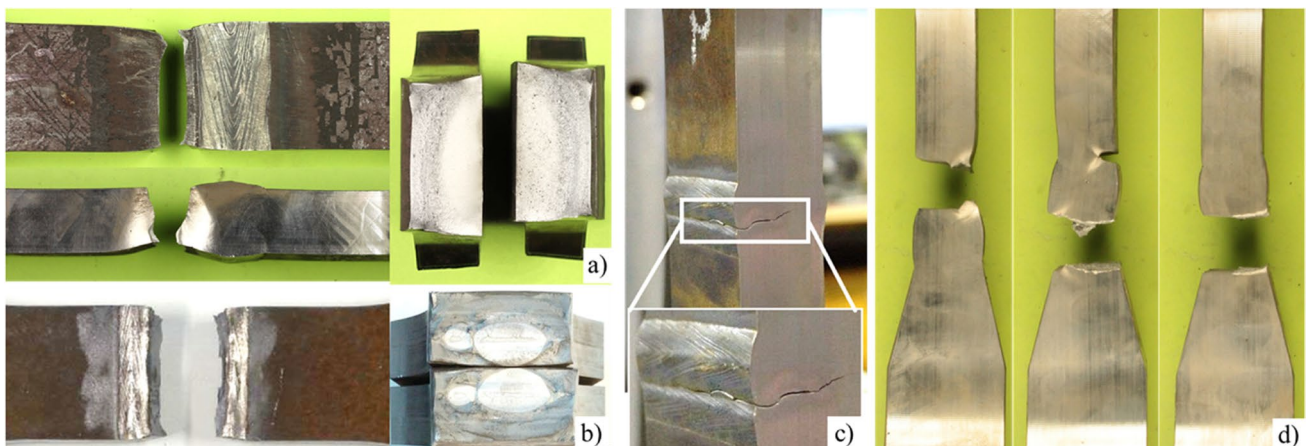
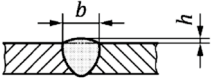
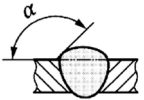
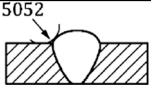
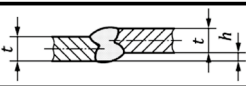
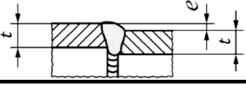



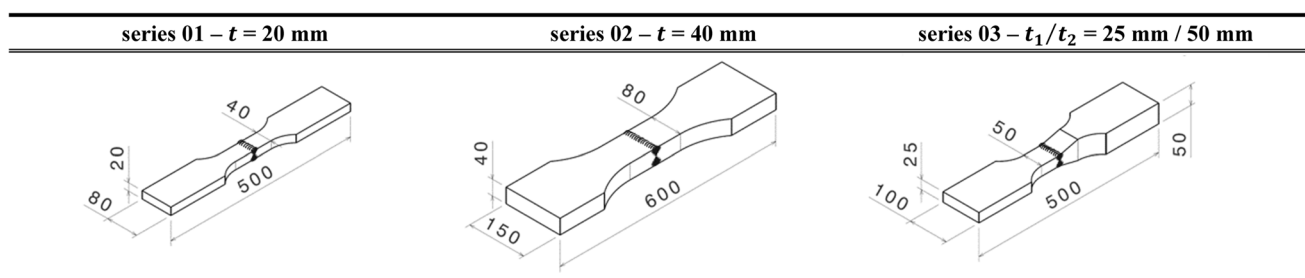
Fig. 4 Different failure modes of specimens with butt-welded joints [2]

**Table 3** Limit values for imperfections of butt-welded joints acc. to ISO 5817 [3]

imperfection	reference acc. to ISO 6520-1	ISO 5817: B (Table 1)	ISO 5817 Annex C: B125
<b>weld overfill <math>h</math></b>			
	502	$h \leq 1 \text{ mm} + 0.1b$ but max. 5 mm	$h \leq 0.2 \text{ mm} + 0.1b$
<b>weld toe angle <math>\alpha</math></b>			
	505	$\alpha \geq 150^\circ$	$\alpha \geq 150^\circ$
<b>weld toe radius <math>r</math></b>			
	5052	-	$r \geq 4 \text{ mm}$
<b>linear misalignment <math>e</math></b>			
	5071	$e \leq 0.1t$ but max. 3 mm	$e \leq 0.05t$ but max. 1.5 mm
	5072	$e \leq 0.5t$ but max. 2 mm	$e \leq 0.5t$ but max. 1 mm
<b>angular misalignment <math>\beta</math></b>			
	508	-	$\beta \leq 1^\circ$

are required for the definition of a FAT-value based on tests. The IIW-Recommendations [8] suggest tests on two stress levels. Failure of the specimen should occur between  $N = 5 \cdot 10^4$  and  $N = 10^6$  load cycles. In comparison, the ISO/TR 14345 [32] defines the requirement for as many tests as necessary for the statistical evaluation, but a minimum of  $n = 8 \dots 10$  samples. Every stress level shall be tested with at least two samples. The regulations according to DVS-Technical Code 2403 [33] require tests on three stress levels with  $n = 3$  samples on each level, whereby the number of load cycles must be  $N < 10^6$ . In addition,  $n = 3$  (better  $n = 5$ ) samples should be tested until  $N = 10^7$  number of cycles. If only a small number of samples ( $n < 10$ ) is available, the tests can be performed with the pearl string method [33]. For tests that shall be representative for a specific quality level (e.g.

quality level B acc. to ISO 5817 [3]) the DVS-Technical Code 2403 [33] states that the samples must be mixed with respect to their weld seam quality. Specimens with similar quality characteristics should not be tested at the same stress level. It is known that the weld toe radius  $r$  and the weld toe angle  $\alpha$  have a significant influence on the fatigue strength in tests. Furthermore, in butt-welded joints secondary bending effects caused by the linear misalignment  $e$  and angular misalignment  $\beta$  affect the fatigue resistance. Therefore, a documentation of the tested specimens with all geometrical parameters of the weld seams is recommended. The ISO/TR 14345 [32] and the DVS-Technical Code 2403 [33] provide some information on this. Furthermore, the mechanical and chemical characteristics of the base materials should be determined by tests.

**Fig. 5** Overview of the butt-welded specimens

### 3.2 Test programme and specimens

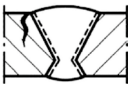
The geometrical dimensions of the small-scaled specimens are shown in Fig. 5. The specimens were manufactured as described in the following. The heavy plates were cut to size using the autogenous flame cutting. The plates received a double-V weld preparation with broad root face for a DV butt weld. According to ISO 9692-2 [34], a weld seam opening angle  $\alpha = 60^\circ$  and a gap of  $b = 4 \dots 6$  mm was set on both sides. For a good weld execution, run-on and run-off pieces were attached. An inverter welding power source from Fa. *Lincoln Electric* was used for joining the plates by the submerged arc welding. The root pass was welded manually using the GMAW process, then overlaid by an SMA process and subsequently ground out before the back run was welded on. The execution of the filler and cover layers was done with the submerged arc welding single wire process in alternating double-sided weld runs. Due to the alternating welding run, the angular misalignment  $\beta$  was largely balanced out. The plates with a thickness of  $t = 40$  mm were preheated to a temperature of at least  $T_p = 100$  °C. The short specimens ( $L = 500$  mm) were cut from the welded plates by saw cut. The specimens with a plate thickness of  $t = 40$  mm were cut by jet cutting. The mechanical processing of the sectional taper was done afterwards.

Table 4 shows the test programme. Specimens with butt-welded joints without systematic linear misalignment  $e$  were tested. Besides of the weld toe radius  $r$ , which was not taken into account in the measurements, most of the small-scaled specimen meet the requirements of the quality level B90 according to ISO 5817 [3]. In addition, some of the samples even satisfy the limits

for quality level B125. The series 01 ( $t = 20$  mm) and 02 ( $t = 40$  mm) were tested at high mean stress level ( $R \geq 0.3$ ). For both series a total number of  $n = 22$  specimens were tested until failure in the high cycle fatigue region. The tests were performed at constant stress levels using the load level method. For this test method, three stress levels ( $n = 5$  specimens on each level) were tested. When selecting the test specimens, care was taken to select them acc. to their weld imperfections. This ensured that their imperfections were suitably represented. The determination of the endurance limit was not part of the study. Specimens with high linear  $e$  or angular misalignment  $\beta$  were tested as runouts at a load ratio of  $R = 0.5$  to secure the design S-N curve. For the tapered specimen without systematic linear misalignment  $e$ , different plate thicknesses  $t_1 = 25$  mm and  $t_2 = 50$  mm were used. The larger plate had a 1:4 chamfer for better load transfer. Due to production-related difficulties, most of the samples had imperfections that did not meet the requirements of quality level B acc. to ISO 5817 [3]. This caused a reduced sample size of  $n = 10$  specimens. These specimens were tested at a load ratio of  $R = 0.1$ .

For the specimen manufacturing, a structural steel S355J2 + N acc. to EN 10025-2 [35] was used. The mechanical properties of this material meet the requirements for the yield  $R_{eH}$  and ultimate tensile strength  $R_m$  according to the standard (Table 5). The surface condition was “as rolled” with a typical surface roughness for mill scale. An additional grit-blasting to achieve a defined surface preparation level was not part of the manufacturing process.

**Table 4** Test programme for structural detail butt-welded joint

series	structural detail	welding process	steel grade	plate thickness $t$ [mm]	load ratio $R$ [-]	sample number $n$ [-]
01		SA (121)	S355J2+N	20	0.3   0.5 <sup>1)</sup>	22
02				40	0.3   0.5 <sup>2)</sup>	22
03				Tapered plates 25/50	0.1	10
sample number $\Sigma$						54

<sup>1)</sup> Runout at  $R = 0.5$

<sup>2)</sup> Fracture or runout at  $R = 0.5$

**Table 5** Mechanical and chemical properties of the base material S355J2 + N

$t$ [mm]	$R_m$ [N/mm <sup>2</sup> ]	$R_{eH}$ [N/mm <sup>2</sup> ]	$R_{eL}$ [N/mm <sup>2</sup> ]	$A_g$ [%]	$KV$ [J]	C [%]	Si [%]	Mn [%]	P [%]	S [%]	N [%]	Cu [%]
20	526	431	386	15.70	226	0.150	0.185	1.24	0.016	0.0039	0.014	0.009
40	544	342	335	14.45	166	0.163	0.202	1.54	0.018	0.0027	0.017	0.031
25	527	391	358	13.97	209	0.176	0.154	1.42	0.015	0.0031	0.018	0.023
50	511	342	335	12.63	138	0.113	0.227	1.34	0.015	0.0078	0.018	0.158

\* $KV$  taken from the 3.1 Inspection certificate and determined at  $T = -20$  °C

In accordance with the note from ISO/TR 14345 [32] or DVS-Technical Code 2403 [33], the specimens were measured and documented with regard to imperfections (Group 5, ISO 6520–1 [36]).

This includes the following:

- Linear misalignment  $e$  (5072 or 5071 acc. to ISO 6520–1 [36])
- Excess weld metal with weld overfill  $h$  (502 acc. to ISO 6520–1 [36])
- Weld toe angle  $\alpha$  (505 acc. to ISO 6520–1 [36])
- Angular misalignment  $\beta$  (508 acc. to ISO 6520–1 [36])

Figure 6 shows an example of a macroscopic image for a specimen of the plate thickness  $t = 20$  mm. The measurement results of the geometrical imperfections for this specimen meet the requirements of the quality level B125 from Table 3, with the exception of the weld toe radius  $r$ . Exemplary macrosections of the different specimens are also shown to illustrate their weld geometries.

A comparison of the allowable and the measured imperfections of the specimens can be seen in Fig. 7. This comparison clarifies that the submerged arc welded specimens comply to the quality level B.

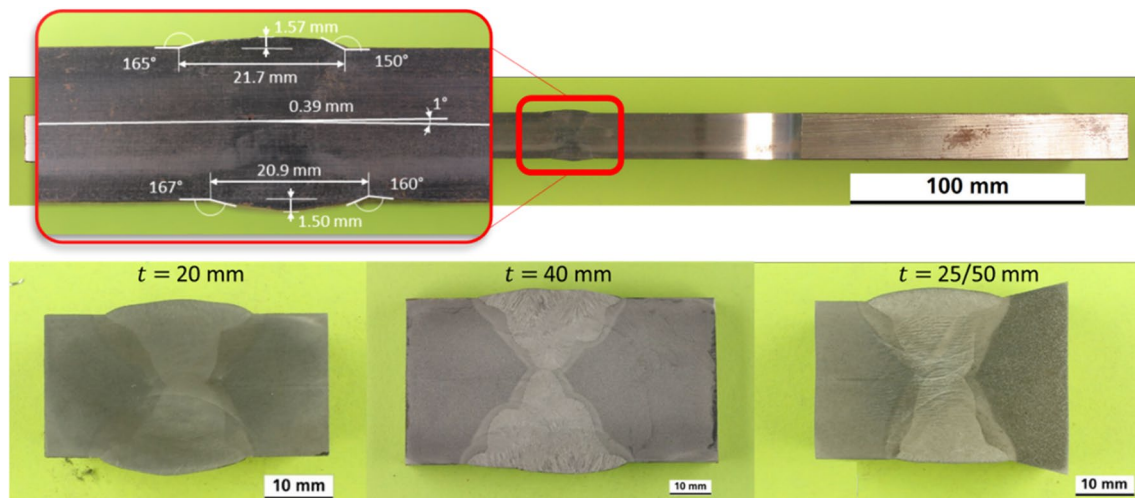


Fig. 6 Macroscopic image for measuring the weld imperfections and macrosections of the weld seams

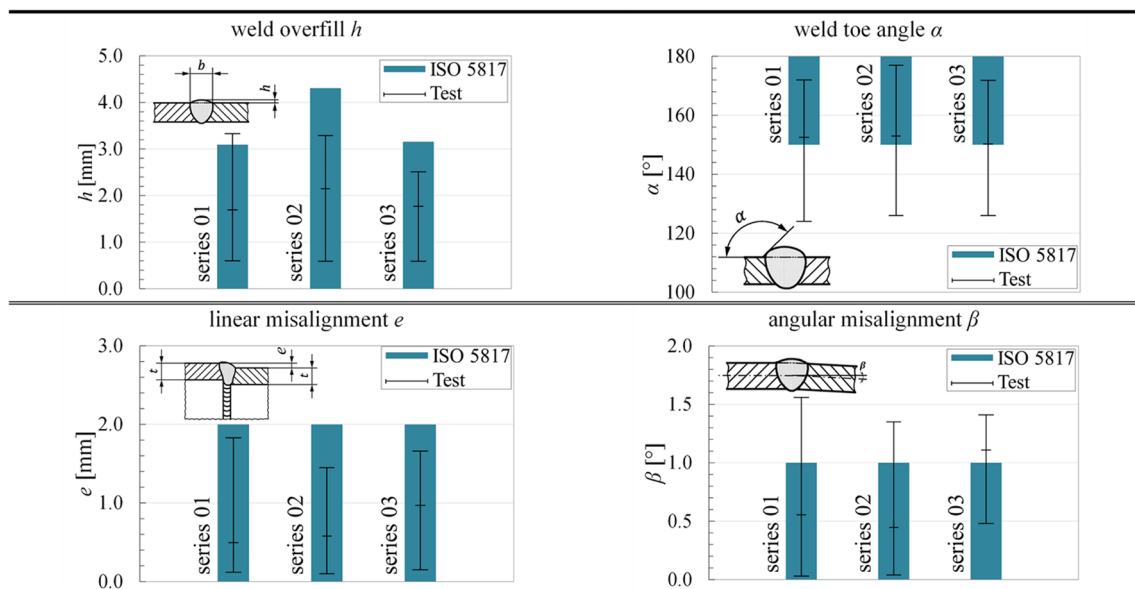
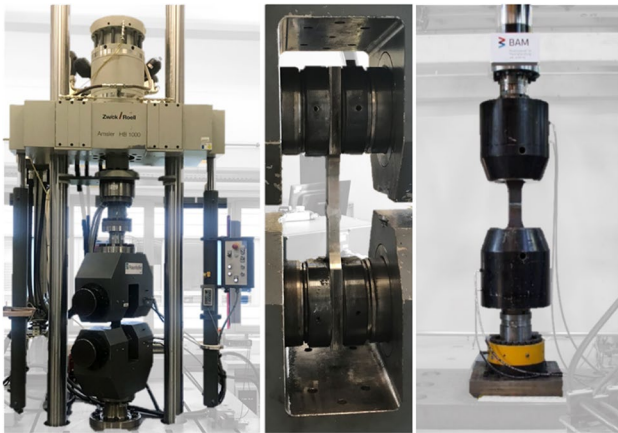


Fig. 7 Comparison of allowable (ISO 5817) and measured imperfections of the tested specimens from series 01 to 03





**Fig. 8** Servo-hydraulic testing machine ZWICK/ROELL HB1000 in the test laboratory of the Fraunhofer IGP and the FORM+TEST at BAM Berlin

### 3.3 Fatigue tests on small-scaled specimens and statistical evaluation

The tests were performed on servo-hydraulic testing machines. Figure 8 shows the servo-hydraulic testing machine Zwick/Roell HB1000 with a specimen of series 01 at Fraunhofer IGP and the testing machine FORM+TEST with a specimen of series 02 at Federal Institute for Material Research and Testing (Bundesanstalt für Materialforschung und -prüfung BAM) Berlin. The fatigue tests were carried out force-controlled with constant amplitude loading. The test stopped if complete fracture of the specimen or a defined number of cycles was reached without failure (=run-out). The test frequencies were between  $f = 12$  Hz and 18 Hz.

For all specimens, crack initiation was observed at the weld toe only.

The test results are statistical evaluated according to the Background Information of the EN 1993–1-9 [37]. For each test series, the characteristic fatigue strength ( $\Delta\sigma_C$ ) is determined, which is defined as the “one-sided confidence interval with a lower limit defining a 95 % probability of survival for log ( $N$ ) test data” [37]. Table 6 contains the results from the statistical evaluation. Furthermore, a separate evaluation is done for a subset of specimens from test series 01 that fulfils the requirement for the higher quality level B125 except for the radius of the weld toe  $r$ .

For test series 01 ( $t = 20$  mm), a value of  $\Delta\sigma_C = 100.97$  N/mm<sup>2</sup> is determined for a constant slope of  $m = 3$ . Based on the test data, the variable slope of the S–N curve leads to an exponent  $m = 3.68$ . The corresponding fatigue strength is then  $\Delta\sigma_C = 111.90$  N/mm<sup>2</sup>. The common standards [7, 8] define a constant slope of  $m = 3$  for welded joints under nominal stress range  $\Delta\sigma$ . Considering the standard deviation of the S–N curve exponent, the standardised slope of  $m = 3$  seems to be justified for this test series as well. The scatter of the number of cycles at one stress level (see Fig. 9a and b) can be explained by the existing imperfections of the specimens. A sufficient representation of the permissible imperfections according to the quality level B of ISO 5817 [3] was given in series 01 (see Fig. 7). Wind turbines are exposed to a high number of cycles  $N$  and low nominal stress range  $\Delta\sigma$  during their service life. For this purpose, additional tests were done to ensure the validity of the design S–N curve of FAT 100 ( $m = 3$ ). Two samples were tested at high load ratio of  $R = 0.5$  with a stress level of 1.5 times the constant amplitude fatigue limit  $\Delta\sigma_D$  related to FAT 100. Both samples reached the predefined maximum number of cycles  $N = 5 \cdot 10^6$  without

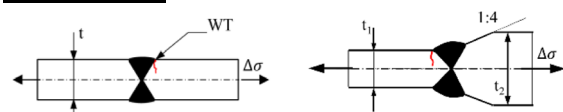
**Table 6** Results from the statistical evaluation according to the background information of the Eurocode 3

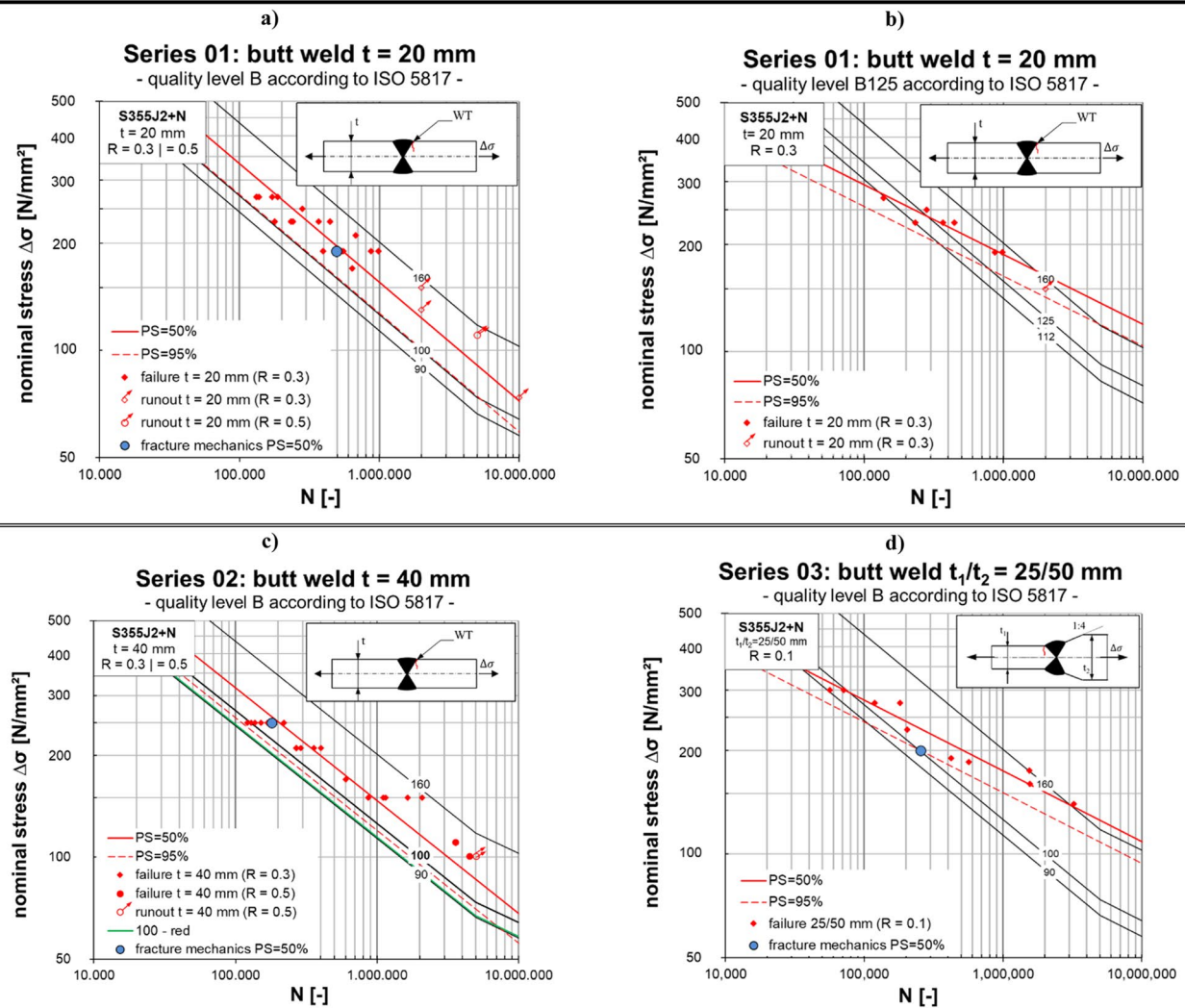
series	welding process	plate thickness $t$ [mm]	$R$ [-]	#data [-]	slope		FAT-value	
					$m = 3$ [-]	$m = \text{var.}$ [-]	$\Delta\sigma_C$ ( $m = 3$ ) [N/mm <sup>2</sup> ]	$\Delta\sigma_C$ ( $m = \text{var.}$ ) [N/mm <sup>2</sup> ]
01	SA (121) <sup>1)</sup>	20	0.3 <sup>2)</sup>	17	3	3.68 <i>0.547</i>	100.97 (123.02)	111.90 (137.31)
01 - B125	SA (121)	20	0.3 <sup>2)</sup>	7	3	5.10	102.79 (130.20)	142.25 (163.27)
02	SA (121) <sup>1)</sup>	40	0.3 <sup>3)</sup>	20	3	3.90 <i>0.191</i>	95.46 (116.68)	116.56 (130.51)
03	SA (121) <sup>1)</sup>	Tapered plates 25/50	0.1	10	3	4.86 <i>0.397</i>	83.24 (121.27)	130.96 (151.17)

**Legend**

- <sup>1)</sup> Imperfection according to quality level B
- <sup>2)</sup> Runout at  $R = 0.5$
- <sup>3)</sup> Runout and fracture at  $R = 0.5$
- B125** – Quality level B125 acc. to ISO 5817 [4]
- (...) values for probability  $P_S = 50\%$
- Italics* – standard deviation of slope parameter

**Structural detail**





**Fig. 9** Classification and statistical evaluation of the samples from series 01 to 03 in the S–N chart for nominal stress range according to the EN 1993–1–9

any failure. Another specimen with extremely linear misalignment ( $e = 1.83$  mm) and sharp weld toe angle ( $\alpha = 148^\circ$ ) survived  $N = 10^7$  number of cycles at a stress level of the constant amplitude fatigue limit  $\Delta\sigma_D = 73.7$  N/mm<sup>2</sup>. Thus, the FAT-class of 100 ( $m = 3$ ) can be considered validated for the intended field of application.

The influence of the plate thickness is the subject of investigation in test series 02 ( $t = 40$  mm). Again, butt-welded specimens were tested at a load ratio  $R = 0.3$  and three stress levels. All failures occurred at the weld toe. This series comprises  $n = 20$  fractured specimens. The statistical evaluation results in a fatigue strength of  $\Delta\sigma_C = 95.64$  N/mm<sup>2</sup> for a constant slope of  $m = 3$ . When considering the thickness reduction factor as required in [7] and [8] by  $k_s = (25/t)^{0.2}$ , the FAT-class 100 from series 01 is reduced to  $\Delta\sigma_{C,red} = 91$  N/mm<sup>2</sup> (see green line, Fig. 9). It can be stated

that the consideration of the plate thickness allows a reliable design. The variable slope of the S–N curve from the statistical evaluation  $m = 3.9$  is slightly flatter. The FAT-class for this variable slope is  $\Delta\sigma_C = 116.56$  N/mm<sup>2</sup>. A comparison of the FAT-classes for a survival probability of 50 % of the two series shows a reduction of the fatigue strength of almost 5 %, as the thickness reduction factor leads to a reduction of 10 %. A closer look on the imperfections of the tested specimens revealed a smaller angular misalignment  $\beta$  for the specimens with larger plate thicknesses  $t$ . The related linear misalignment ( $e/t$ ) for the specimens with smaller plate thickness is 2.1 %. The thicker specimens ( $t = 40$  mm) have only 1.35 %. The linear misalignment  $e$  is limited to  $e \leq 3$  mm (5071) or  $e \leq 2$  mm (5072). For this reason, the fatigue strength reducing effect of the linear misalignment  $e$  is likely to diminish



with larger plate thicknesses  $t$ . A detailed examination of this issue will be carried out in the numerical investigations.

Figure 9b shows a subset ( $n = 7$ ) of series 01. These specimens meet the higher requirements of quality level B125 according to ISO 5817 [3]. Excluded from this assessment is the weld toe radius  $r$ . The variable slope from the statistical evaluation flattens out to  $m = 5.1$ . The FAT-class for this slope is  $\Delta\sigma_C = 142.25 \text{ N/mm}^2$  for a survival probability of 95 %. The increase in fatigue strength allows the assumption that especially the linear misalignment  $e$  and the angular misalignment  $\beta$  are sensitive to the fatigue resistance of the tested plate thickness  $t$ . Higher quality levels seem to flatten the S–N curve. An evaluation of the fatigue resistance only based on the consideration of the linear misalignment  $e$  by SCF's cannot provide generally valid statements for a reliable design. This is due to the mutual influence of the individual parameters from the weld seam geometry. Therefore, it is recommended to generate a database which covers manufacturing-typical characteristics related to weld imperfections.

In series 03, the influence of a chamfer on the fatigue resistance was investigated. For this purpose,  $n = 10$  tapered specimens ( $t_1/t_2 = 25/50 \text{ mm}$ ) were tested with a constant load ratio of  $R = 0.1$ . The tested specimens have the largest linear  $e$  and angular misalignment  $\beta$  compared to those without chamfer from series 01 and 02. Because of this, the specimens from series 03 are characterised by a sharp weld toe. The measurement of the weld seam geometry delivered weld toe angles  $\alpha$  less than  $150^\circ$ . As a result, the fatigue failure mostly occurred on the side of the thicker plate. The statistical evaluation shows a FAT-class of  $\Delta\sigma_C = 130.96 \text{ N/mm}^2$  with a survival probability of 95 %. In chapter 3.1, it was pointed out that for small load ratios  $R$  the S–N curve flattens and higher values of fatigue strength are achieved. Even if a reduction of 20 % according to IIW-Recommendations [9] is applied on the experimentally determined FAT-class, because

the load ratio was smaller than 0.5, the test series would still result in a FAT-class 100 ( $m = 3$ ) for butt-welded joints with a 1:4 chamfer on both sides. In summary, it can be stated that the submerged arc welding process results in higher quality levels of welded joints compared to manual welding. The measured weld overfills  $h$  were below the normative limits. It must also be noted that the linear misalignment  $e$  and angular misalignment  $\beta$  are dominant parameters regarding the fatigue strength of butt-welded joints. Nevertheless, for butt-welded joints produced with the submerged arc welding process, a classification into the next higher FAT-class 100 seems possible. This classification is linked to the limits of quality level B, which must be complied with.

### 3.4 Fatigue tests on large components with butt-welded joints

To evaluate the transferability of the observed results from the fatigue tests performed on small-scaled specimens, additional fatigue tests were carried out on the component level. Such investigations are considering structural influences resulting from manufacturing procedures as well as from the specific bearing behaviour of the component itself. Residual stresses from manufacturing due to the high stiffness of the components and larger imperfections are some important effects. The objective of the large component tests is to validate positive effects of the high weld quality of submerged arc welding on the structural detail butt-welded joint also on the component level. The component tests were carried out at the Federal Institute for Materials Research and Testing (BAM) in Berlin, Germany (see Fig. 10). Also shown in Fig. 10 are some specimens before testing.

The choice of the specimen geometry is defined by different boundary conditions. The specimens should be representative for typical butt welds in wind turbine tower



Fig. 10 Test rig at BAM Berlin for fatigue tests on tubes with butt-welded joints, geometry of the specimens, and position of strain gauges

segments, both in terms of structural detail as well as to the manufacturing process. Furthermore, the comparability to the fatigue tests on small-scaled specimens must be ensured, and finally, the possibilities of the test facility have to be considered. Based on these parameters, butt-welded tubes are chosen with a geometry given in Fig. 10. In this test series 04,  $n = 4$  component specimens are tested. As tube material a S355J2+N was used. The butt weld was executed as double-V-butt by submerged arc welding from inside with an additionally weld from the outside. Both ends of the welded tube were closed with steel plates due to allow measuring of an applied inner air pressure as an additional crack indicator. The specimens were manufactured by a construction company active in the area of manufacturing wind energy structures. Thereby, realistic manufacturing conditions of the specimens were ensured. A summary of the test programme is given in Table 7.

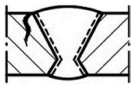
At all specimens the geometrical imperfections were documented from the outside before testing. The weld imperfections have to meet the requirements of quality level B acc. to ISO 5817 [3]. For this purpose, the plate thicknesses  $t$ , tube diameter  $D$ , weld bead width  $b$ , weld overfill  $h$ , and linear misalignment  $e$  were determined by ultrasonic and a 3D-scan of the weld seam surface. The results from this 3D-scan and general measurement are summarised in Table 8. It was not possible to document the weld condition on the inside of the tubes. But it can be stated that weld bead width  $b$  and weld overfill  $h$  were generally larger compared to the outside conditions due to the defined welding procedure.

For the fatigue tests, a four-point bending configuration was chosen as illustrated in Fig. 10. With this configuration, a constant bending moment was generated in the middle area of the specimen where the butt weld was located.

A servo-hydraulic test cylinder with a maximum load of 1600 kN and a test frequency of  $f = 0.7$  Hz was used. For the tests, a vertical compression load was applied on the specimens. This results in tensile stresses at the bottom side of the horizontal tube. Both lower supports of the specimen were movable on rolls to avoid additionally stresses from any constrains. During the tests the applied load, the vertical displacement as well as the load cycles were measured. Additionally, it was intended to observe the crack initiation and the breakthrough event. Therefore, the applied inner air pressure (0.5 bar) of the tube was measured to detect a breakthrough event. Strain gauges were applied on the outside to measure nominal strains (stresses) as well as structural strains (stresses) during the tests as illustrated in Fig. 10.

Comparable to the fatigue tests on small-scaled specimens, the component tests were carried out force-controlled with constant amplitude loading and a load ratio of  $R = 0.3$ . Two stress levels were chosen based on the results of the fatigue tests on small-scaled specimens. The determination of the belonging target load level was done over the measured nominal strains of the strain gauges (see Fig. 10) by static preloading tests. To reduce effects of residual stresses, the target load was applied several times before the cyclic test load was finally defined. Stresses resulting from the dead weight of the tube and the load application system were determined before any load application and finally considered in the calculation of the loads for the cyclic test. For the detection of crack initiation, the deviation of the strain measurements of the strain gauges was used. The breakthrough event was detected by the pressure loss of the inner air pressure of the specimen, which was used as result for the number of cycles. This definition is comparable to the failure definition of the fatigue tests on small-scaled

**Table 7** Test programme for structural detail transverse butt-welded joint on component level

Series	Structural detail	Welding process	Steel grade	Plate thickness $t$ [mm]	Load ratio $R$ [-]	Sample number $n$ [-]
04		SA (121)	S355J2+N	17.5	0.3	4

**Table 8** Overview of measured geometrical values of specimen outside before testing

Specimen	Diameter left $D_{\text{left}}$ [mm]	Diameter right $D_{\text{right}}$ [mm]	Plate thickness left $t_{\text{left}}$ [mm]	Plate thickness right $t_{\text{right}}$ [mm]	Weld overfill $h$ [mm]	Weld bead width $b$ [mm]	Linear misalignment $e$ [mm]
01	659.9	660.2	17.27	17.31	1.65	29.8	-0.40
02	662.2	662.9	17.09	17.40	1.52	29.9	-0.35
03	661.0	659.4	17.19	17.18	1.60	26.2	0.09
04	660.4	659.8	17.32	17.42	1.70	28.2	0.49

specimen where the fracture of the specimens was used. The fatigue test was finally stopped after reaching a certain value of vertical displacement. Crack initiation took not place at the outer surface of the tubes in all tests. The strain measurements indicate instead crack initiation at the inner surface of the tube near the weld toe of the butt weld. However, due to the major relevance of the breakthrough event, this information was sufficient for a rough detection of the crack initiation point. On the contrary, the breakthrough event was clearly detected by the air pressure loss, which was additionally confirmed by video observation of the weld. In Fig. 11, the measurements for crack initiation by strain gauges and breakthrough by air pressure are illustrated for specimen number 2. The decrease of strain indicates that the fatigue crack took place in front of the strain gauge at the inner tube surface at right side of the weld. The opposite weld side remains unaffected until shortly before the breakthrough.

The final state of the fatigue crack is shown exemplarily in Fig. 11 for specimen number 2. It was similar for the other three specimens. Figure 12 points out that the results of the component tests fit well into the scatter range of the small scaled specimens of the plate thickness  $t = 20$  mm. Here, the number of load cycles at the breakthrough event was used for the comparison. The component results confirm the classification of the structural detail in FAT 100. Based on the location of the results from component tests, a flatter slope of the S–N-curve than  $m = 3$  seems not to be appropriate.

## 4 Numerical studies using the FEM

### 4.1 Effective notch stress concept

In addition to fatigue testing on butt-welded joints, numerical simulations are carried out. These are used to analyse the interaction between the imperfections of the weld geometry and the expected fatigue strength in more detail. For this

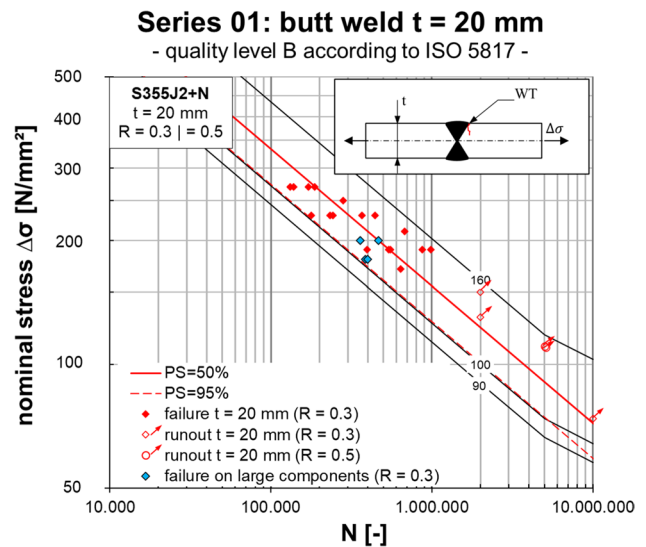


Fig. 12 Classification of test results from large component tests of series 04 into the scatter range of the small scaled tests of test series 01

purpose, considerations are made acc. to the effective notch stress. The effective notch stress concept allows to consider the real weld geometry. The aim of this study is to show that a higher fatigue resistance from the fatigue tests on butt-welded specimens is directly linked to the higher quality level of the weld seam geometry. Further, this analysis is extended to a tower segment.

#### 4.1.1 Boundary conditions for the FE analysis of butt-welded specimen

In a first step, the results from the numerical simulation should be compared to the results from the fatigue tests. The goal here is to work out the influence of the local geometric quality on the expected value of the stress concentration

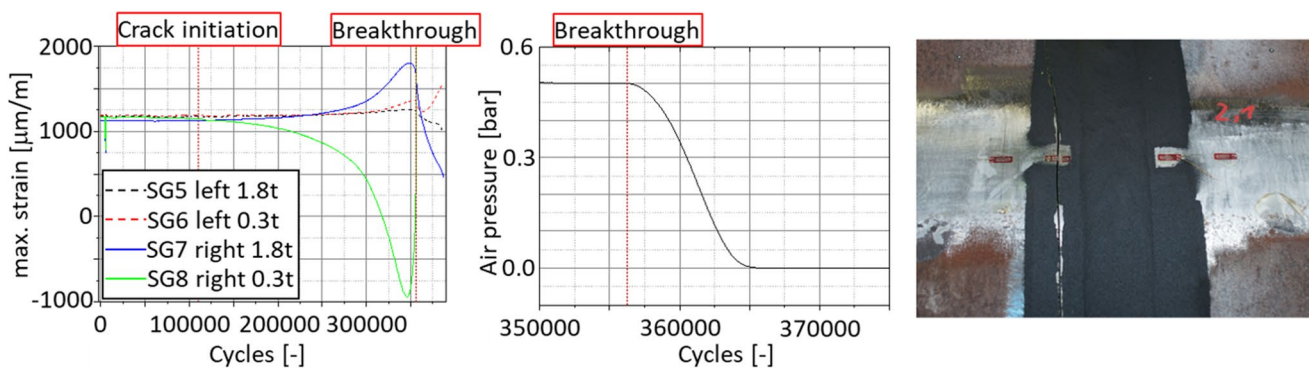
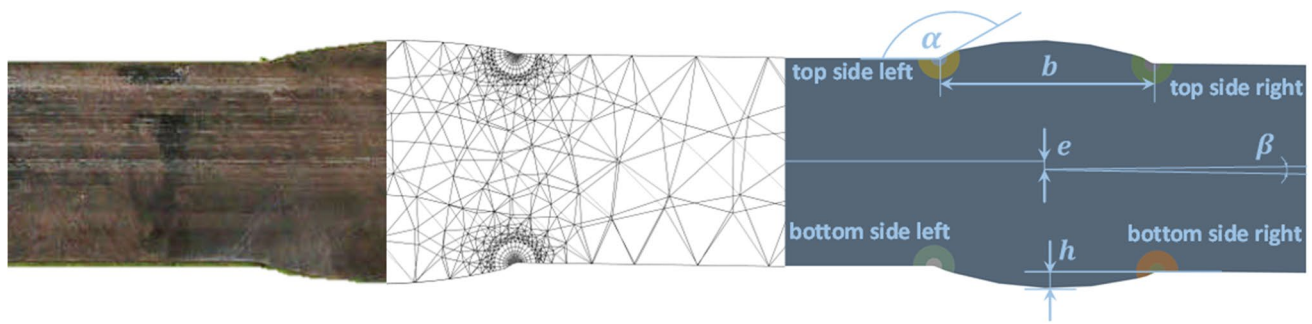


Fig. 11 Strain measurement for crack initiation (left), air pressure development for breakthrough event at specimen number 2 (middle) and image of final crack location at specimen number 2 (right)



**Fig. 13** Transfer of the real weld seam geometry from macroscopic measurement into FE model

factor  $K_t$ . For this study, the real geometry of the weld seam from macroscopic measurement is used as input parameter for the numerical model. Figure 13 shows an example of the weld seam geometry approximated by the mesh and the geometry parameters of the weld seam.

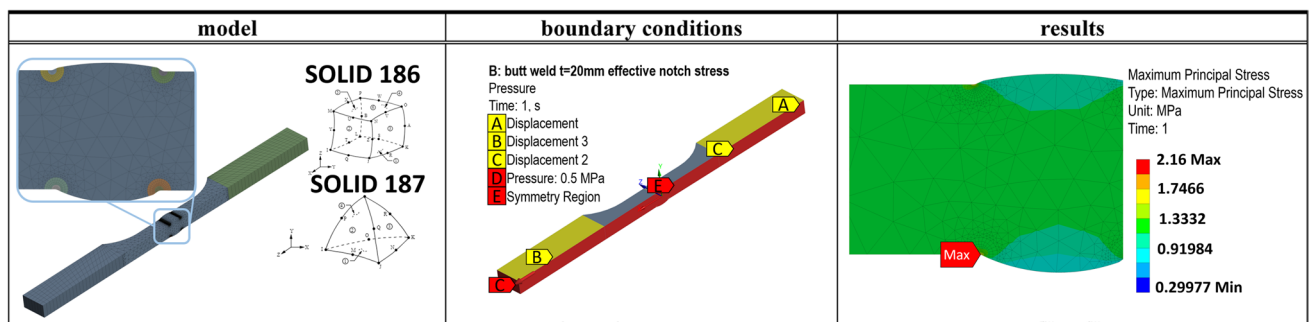
For analysis a 3D model of the specimen was created in ANSYS2021 R1. This allows to consider the real installation situation in the testing machine. An overview of the boundary conditions of the FE model is given in Fig. 14.

The verification according to the notch stress concept is generally considered to be computationally time and capacity intensive with a high modelling effort. For a better efficiency of the numerical simulation, a fully parameterized half-model was built up. This resulted in the use of the symmetry boundary condition (boundary condition E) on the sectional plane. The width to thickness ratio in the critical net cross-section was set to  $b/t = 2$  for all specimen geometries. This was realised by cross-sectional tapering of the specimens. Applying a unit load (boundary condition D) as a pressure of  $p = -0.5$  MPa on the end face of the specimen results in a nominal stress of  $\sigma_n \approx 1$  MPa in the nominal cross-section. Through this setting, the value of the maximum principal stress at the weld toe can be directly assumed as the effective notch stress  $\sigma_e$ . The test setup in the testing machine was modelled by using a boundary condition which blocked the displacement in global Y-direction (boundary

condition B & C) of clamping area. To achieve a statically determined system the displacement of the end face of the specimen was blocked in global X-direction by an additional boundary condition (boundary condition A). The material behaviour was chosen to linear elastic with an elasticity modulus of  $E = 210,000$  MPa and a Poisson's ratio of  $\nu = 0.3$ . Based on the modelling specification acc. to the DVS-Technical Code 0905 [18] for the effective notch stress concept, the weld toe was rounded by a fictitious radius of  $r_{ref} = 1$  mm. The settings for the local mesh at the weld tip also met the requirements of the DVS-Technical Code 0905 [18] and the IIW-Recommendations [8]. Thus, the correct determination of the effective notch stress can be ensured. For the meshing of the geometry, only solid elements with quadratic displacement function were used (SOLID 186 & 187). The parameters of the real weld geometry vary over the length and width of the weld. By using the results from a 2D macroscopic measurement of the cross-sectional weld seam geometry, an idealised assumption was made by the authors.

#### 4.1.2 Evaluation of the FE analysis of butt-welded specimens

For the evaluation of the results obtained from the numerical simulations, the nominal stresses levels from the tests are



**Fig. 14** Overview of the FE model of the butt-welded specimen



multiplied by the value of the stress concentration factor  $K_t$  giving the notch stress  $\sigma_e$ , and then presented in an S–N chart together with the number of load cycles  $N$  achieved in the fatigue tests. In addition, the S–N curve FAT 225 for welded steel joints acc. to the effective notch stress concept is plotted in the diagram for the comparison with the tests results. The results for series 01 to 03 are shown in Fig. 15. In 34 of 47 cases, the locations of highest notch stress from the FE analysis matches with the fracture locations from the fatigue tests. For the remaining specimens, the difference between the notch stresses at the location of highest notch stress and the fracture location amounts to a maximum of 10%. Therefore, it can be said that there are competing types of fracture locations. One possible reason for the deviation can be seen in the method to determine the imperfections through a macroscopic cross-sectional image. These images do not capture the entire weld seam geometry along the specimen width.

Most of the test results are above the S–N curve of FAT 225. Only a few specimens of series 02 ( $t = 40$  mm) in the high stress range area are lying below the S–N curve, which would lead to an uncertain statement about the fatigue resistance for these specimens. Nevertheless, it can be positively emphasised that a safe design is possible if knowledge of the seam geometry exists so that the notch stress concept can be safely applied. Therefore, a possibility of a fatigue strength verification based on 3D scans of the weld geometry is given. Conversely, the fatigue strength of welded joints can be adjusted via compliance with permissible limit values.

### 4.1.3 Boundary conditions for the FE analysis of butt-welded joints in tower sections

The sensitivity of the local weld geometry on the expected fatigue resistance of butt-welded joints in tower structures is considered in an additional FE analysis using ANSYS2021 R1. For this purpose, the existing geometric irregularities of butt welds in the tower segment were considered. The numerical study includes the parameters listed below:

- Weld overfill  $h$  [mm]
- Weld toe angle  $\alpha$  [°]
- Linear misalignment  $e$  [mm]
- Weld bead width  $b$  [mm]

For each plate thickness  $t$ , a basic parameter set is used, which are shown in Table 9. During the parameter study, just one of the geometrical parameters was varied. The other parameters were kept constant according to the specifications in Table 9. The parameters were varied within the permissible limits of the quality level B acc. to ISO 5817 [3].

Again, a parametric 3D model is used. An overview of the boundary conditions in the model is shown in Fig. 16. Compared to the FE model of the specimen, a partial tower section is generated by rotating the weld geometry with a radius of  $R = 1,500$  mm. This radius is defined as the distance between the rotation axis and the tower shell centre plane. As similar to the FE model of the specimen, a nominal stress of  $\sigma_n \approx 1$  MPa in the tower shell is generated by a pressure of  $p = -1$  MPa (boundary condition D). This allows the effective notch stress  $\sigma_e$  to be determined directly.

For an optimization of the computational time, a rotation symmetry (boundary condition A) is defined in the model. The radial displacement of the tower section is left free. The load application on the section is realised by a boundary condition B & C which suppresses the displacement in global X-direction at the end face. Also, in this model, linear-elastic material behaviour ( $E = 210,000$  MPa,  $\nu = 0.3$ ) is assigned. The discretisation of the tower geometry is done

Table 9 Overview of the basic parameter sets for the FE analysis

Plate thickness $t$ [mm]	Weld overfill $h$ [mm]	Weld toe angle $\alpha$ [°]	Linear misalignment $e$ [mm]	Weld bead width $b$ [mm]
20	1.75	155	0	20
40	2.0	155	0	40
60	2.5	155	0	60

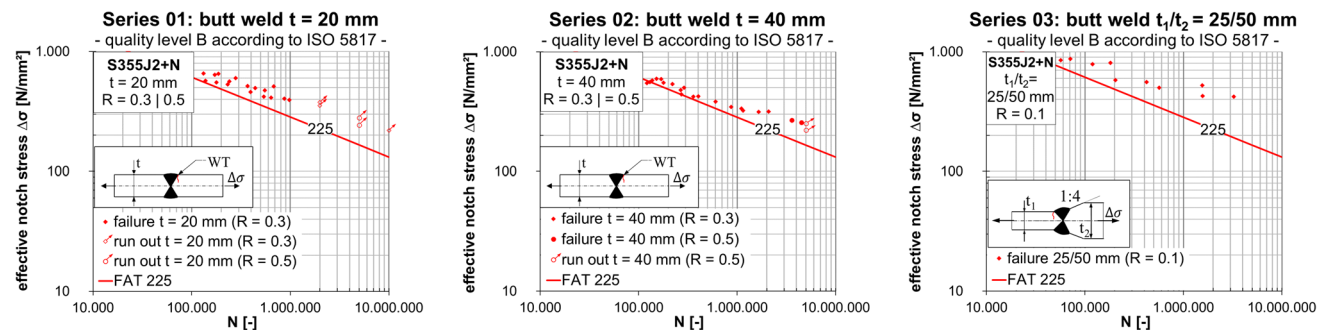


Fig. 15 Comparison of the test results from fatigue tests based on effective notch stresses and the S–N curve of FAT 225

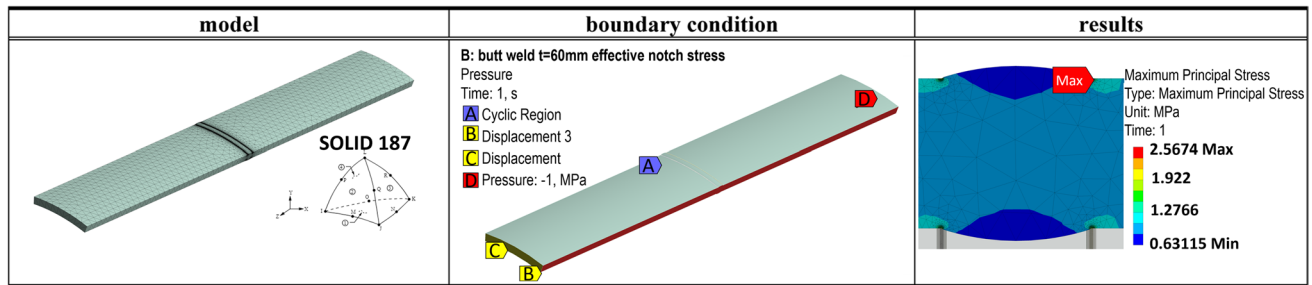


Fig. 16 Overview of the FE model of transversal butt weld in tower section

with a mesh of SOLID 187 elements which have a quadratic displacement function. The DVS-Technical Code 0905 [18] does not contain a recommendation of the reference radius for plate thicknesses greater than 50 mm. Therefore, a reference radius  $r_{\text{ref}} = 1$  mm and the belonging S-N curve with FAT 225 is used for all plate thicknesses  $t = 20 \mid 40 \mid 60$  mm. For tower sections of wind turbines, plate thicknesses larger than  $t = 50$  mm are highly relevant. However, the upper limit of the scope of DVS-Technical Code 0905 [18] is limited in this respect. Other approaches like the nominal stress or the structural hot-spot approach can be used, but do not consider the weld seams geometry. As a result, the local geometry of the weld seams has no influence on the results of the fatigue resistance.

#### 4.1.4 Evaluation of the FE analysis on the structural detail butt-welded joints in tower sections

Figure 17 shows the results from the numerical analysis on the fatigue resistance of butt-welded joints in tower sections by the effective notch stress approach. In addition, the allowable limits for the imperfections of butt-welded joints acc. to ISO 5817 [3] are presented. This illustration highlights the fact of a decreasing fatigue resistance when the imperfection gets close to the permitted limits. This is state of the art [38]. A more differentiated view on the influence of the different imperfections can be found by a comparison of the diagrams. The weld bead width  $b$  is a parameter which has a minor influence on the fatigue resistance. All values of the allowable stress range are on the same level independent on the weld bead width  $b$  and plate thickness  $t$ . For all other parameters, a significant influence on the fatigue resistance is found. The parameters weld toe angle  $\alpha$  and weld overfill  $h$  are less affected by the plate thickness  $t$ . In contrast, the parameter linear misalignment  $e$  shows a high dependence on the plate thickness  $t$ . This interaction is caused by the resulting secondary bending effects. A larger plate thickness  $t$  is less effected by an increasing linear misalignment  $e$  than a small plate thickness. This is shown by the crossing graphs of different plate thicknesses in Fig. 17.

The geometrical parameters of weld seams are correlative. The parameter study with a fixed parameter set and variation of only one parameter does not allow a consideration of the full interaction between the different geometrical parameters. For clarification, a multiple regression can be used. The entire parameter area and the FAT-class are used for this regression. As a result, Eq. (8) could be found. By comparing the coefficients of the different geometrical parameters, the weld toe angle  $\alpha$  and the ratio of  $e/t$  are the relevant parameters. The weld toe angle  $\alpha$  is directly linked to the parameter weld overfill  $h$ . With a correlation coefficient of  $R^2 = 0.9508$ , a good accuracy of the equation can be assumed. The standard error for the FAT-class with  $\sigma(\hat{\vartheta}) = 2.509$  MPa is moderate.

$$\text{FAT} = -40.44 - 390.94 \frac{e}{t} + 0.086b - 8.8h + 1.07\alpha \quad (8)$$

#### 4.2 Fracture mechanics

Besides of the assessment in respect to fatigue by effective notch stress concept, fracture mechanics gains more and more attendance. This required additional measurements of the real geometry of the weld profile. So, the weld toe radius  $r$  was measured at  $n = 10$  specimens of the series 01 by macroscopic images (see Fig. 18).

In the considered area, radii of  $r = 0.14 \dots 3.94$  could be measured. Most of the individual measured values as well as the mean of  $r = 1.23$  are close to the reference radius of  $r = 1$  mm used for the effective notch stress concept. This radius coincides also with measured results from the real tower structure (see Fig. 20). For this reason, a radius of  $r = 1$  mm was chosen for the numerical simulations. The input parameters for the FE simulations of the small-scaled specimen and full-size tower segment are listed in Table 10.

For the fracture mechanics calculation, the most important input is the distribution of the first principal stress along the anticipated crack path. Since the initial crack depth is defined as  $a_i = 0.1$  mm, a



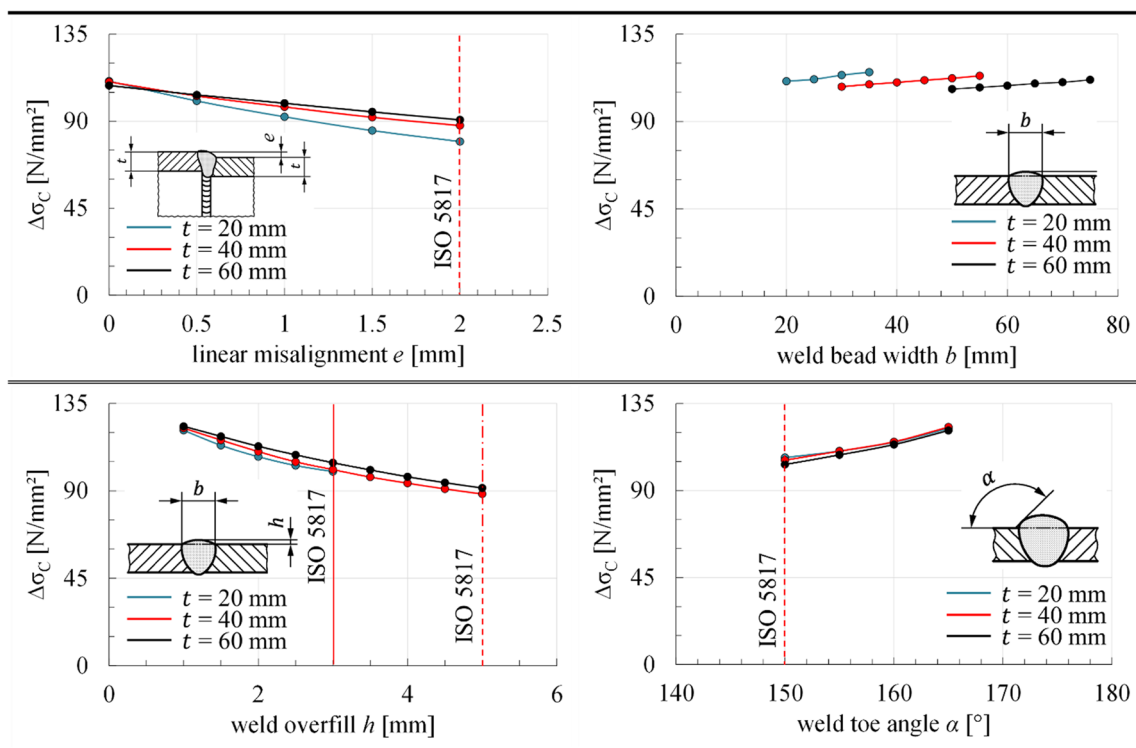


Fig. 17 Results from the parametrical study on the structural detail transversal butt welds in tower section

Fig. 18 Macroscopic measurement of the weld toe radius  $r$  on the butt weld test specimen  $t = 20$  mm

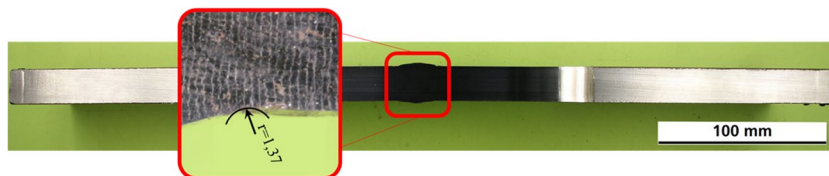


Table 10 Overview of the input parameters for determining the stress gradient

Plate thickness $t$ [mm]	Weld overfill $h$ [mm]		Weld toe angle $\alpha$ [°]				Linear misalignment $e$ [mm]	Angular misalignment $\beta$ [°]	Weld bead width $b$ [mm]	
	Above	Below	Above left	Above right	Below left	Below right			Above	Below
20	1.43	1.70	152	155	158	156	0.36	0.35	20.06	21.67
40	2.73	1.97	154	156	155	149	0.57	0.48	36.63	33.85
25/50	1.73	1.81	147	153	152	149	0.97	1.11	21.05	22.05
60 <sup>1)2)</sup>	3.48		140	153	153	140	1.92	-	60.02	
80 <sup>1)2)</sup>										

<sup>1)</sup>FE model, tower segment

<sup>2)</sup>Weld scan

Selected weld toe radius  $r = 1$  mm

very fine meshing near the surface was necessary, deeper down that may be coarser. Figure 19 shows the stress distribution at the specimen of  $t = 20$  mm plate thickness.

It should be mentioned that the weight function procedure leads to an improper integral, which needs very small steps near the surface.

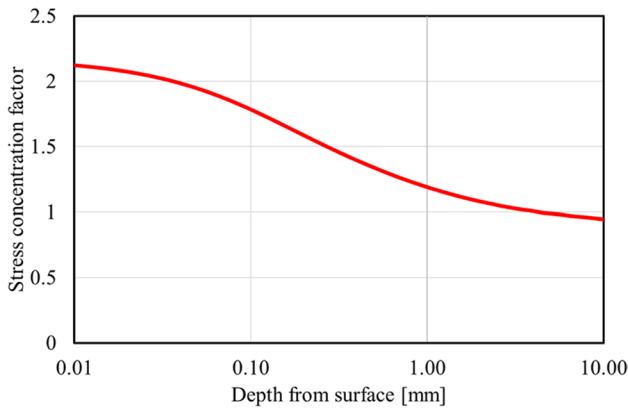


Fig. 19 Stress distribution by FEA

Calculation of number of cycles  $N$  from stress distribution  $\Delta\sigma(x)$  and weight function  $h(x, a)$

$$N = \frac{1}{C_0} \cdot \int_{x=a_0}^{x=a_f} \frac{dx}{\left[ \int_{x=0}^{x=a} \sigma(x) \cdot h(x, a) \cdot dx \right]^m}$$

According to IIW-Recommendations [8], the following parameters have been used (see Table 11).

Table 12 shows the calculated results, derived from stress distributions and a characteristic value of the material constants  $C_0 = 3.0 \cdot 10^{-13}$  and  $m = 3.0$ .

A comparison between the experimental results from Table 6 and Fig. 9 shows a good agreement with the fracture mechanics calculation from Table 12. The favourable behaviour of the large specimens is since

the imperfections become relatively smaller as the plate thickness increases.

### 4.3 Submerged arc butt-welded joints in the manufacturing of tower sections

The determination of weld seams imperfections during the manufacturing process is a challenge for the manufacturer. However, this is a necessary condition for factory production control. An economical solution is offered by 3D measurements of the weld seams geometry with subsequent computer-aided, algorithmic evaluation. The points where particularly strong curvatures occur can thus be localised and used as candidates for further algorithms. This method was used to determine the imperfections for a butt weld in tower section with an outer diameter of  $D \approx 7,700$  as shown in Fig. 20. The determined imperfections include the weld bead width  $b$ , weld toe angle  $\alpha$ , weld toe radius  $r$  on the left and right side of the weld seam, weld overfill  $h$ , and the linear misalignment  $e$ . The measured imperfections include results from  $n = 20$  equidistant section profiles with a distance of  $s = 64$  mm on the circumference of the three-dimensional data set of the weld. The basis of the calculation is the determination of the curvature along the section profile. The total measured distance corresponded to approximately 1.28 m with one section profile determination per  $1^\circ$ . The choice of a suitable resolution of the profile in the recording process has a decisive influence on the accuracy of the results.

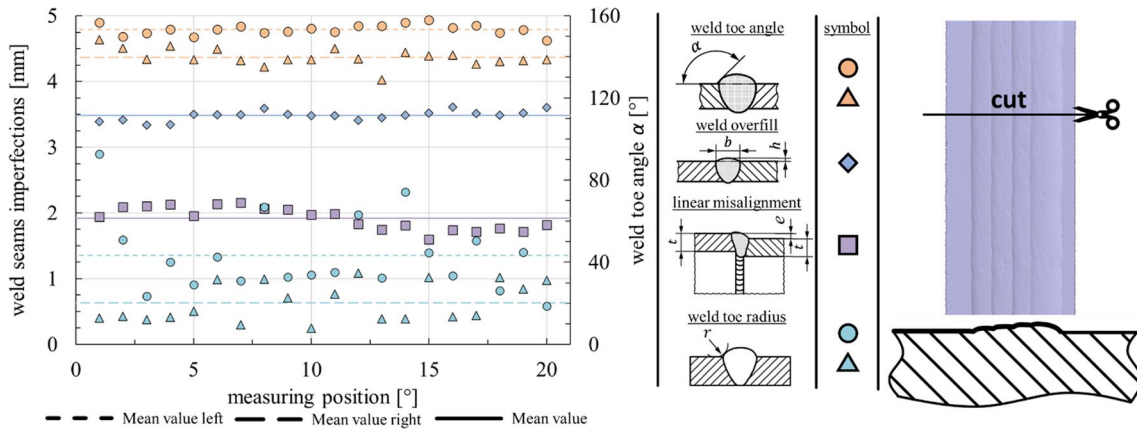
The results of the scan primarily show above all the good and reproducible weld seam quality of the submerged arc welding process. Nevertheless, some individual results of the linear misalignment  $e$  and weld toe angle  $\alpha$  exceed the limit for

Table 11 Parameter set of the fracture mechanics calculation

<b>Crack depths</b>	<ul style="list-style-type: none"> <li>• Equivalent initial crack <math>a_i = 0.1</math> mm</li> <li>• Final crack <math>a_f = t/2</math></li> </ul>
<b>Material constants</b>	<ul style="list-style-type: none"> <li>• <math>C_0 = 1.8 \cdot 10^{-13}</math> [N; mm] (experimental mean) [10]</li> <li>• <math>C_0 = 3.0 \cdot 10^{-13}</math> [N; mm] (characteristic value) [25]</li> <li>• <math>m = 3.0</math></li> </ul>
<b>Toughness</b>	<ul style="list-style-type: none"> <li>• <math>K_{mat} = 5600</math> N mm<sup>-3/2</sup></li> <li>• Estimation by SANZ and WALLIN for S355J2 at <math>T = 20</math> °C</li> </ul>

Table 12 Results from the fracture mechanics calculation by stress distribution and weight function

Series	Plate thickness $t$ [mm]	Stress range $\Delta\sigma$ [N/mm <sup>2</sup> ]	Load ratio $R$ [-]	Linear mis- alignment $e$ [mm]	Angular misalign- ment $\beta$ [°]	Number of cycles $N$ [-]	FAT-value [N/mm <sup>2</sup> ]	
							$P_S = 50\%$	$P_S = 97.7\%$
01	$t = 20$ mm	190	0.3	0.36	0.35	492,000	119	99
02	$t = 40$ mm	250	0.3	0.57	0.48	180,000	112	92
03	$t_1/t_2 = 25$ mm/50 mm	200	0.1	0.97	1.11	244,000	101	84
-	$t = 60$ mm	200	0.5	1.92	0.00	280,000	104	88
-	$t = 80$ mm	200	0.5	1.92	0.00	300,000	106	90



**Fig. 20** Results for imperfect shapes and dimensions (left) and top-view on CAD model with illustrated cross-section from a 3D weld seam scan (right) [39]

the quality level B of the ISO 5817 [3]. These two quantities were found to be particularly sensitive to the fatigue strength in the previous investigations. For this reason, additional numerical and fracture mechanics analysis were carried out to predict the fatigue resistance. For this purpose, the mean values of the individual results from the weld seam scan were transferred to the parametric model of the tower section. This allows the determination of the effective notch stress  $\sigma_e$  and the stress along the anticipated crack path (see Table 13).

### 5 Comparison of normative requirements with experimental and numerical results

The use of the fully mechanised submerged arc welding process in the manufacturing of towers for wind turbines enables the production of welded joints with high execution quality and reproducibility. In conjunction with the increasing execution quality by complying with imperfection limits,

the fatigue resistance of butt-welded joints can be increased. This increase is not yet covered by technical standards but has been demonstrated in experimental studies. A comparison was made between the experimentally determined FAT-classes and those determined by numerical simulation and application of the local approaches. In the latter verifications, the real weld seam geometry was considered. Finally, the results were also compared with the specifications according to the technical standards (Eurocode 3, IIW-Recommendations, DNVGL-RP-C203). Table 13 was prepared for this purpose.

The FAT-classes from the fatigue tests on butt-welded specimens of the same plate thickness are  $\Delta\sigma_C = 100.97 \text{ N/mm}^2$  ( $t = 20 \text{ mm}$ ) and  $\Delta\sigma_C = 95.46 \text{ N/mm}^2$  ( $t = 40 \text{ mm}$ ). The FAT-classes from the calculation according to the crack propagation or the effective notch stress concept provide comparable results. From this, it can be deduced that butt welds with higher weld seam quality have a higher fatigue strength compared to the value from the technical standard with a FAT-class of  $90 \text{ N/mm}^2$ .

**Table 13** Comparison of FAT-classes from experiment, technical standards and the application of the effective notch stress and fracture mechanic concept

Series	Plate thickness $t$ [mm]	Weld bead width $b$ [mm]	Experiment FAT [N/mm <sup>2</sup> ]		Calculated prediction FAT [N/mm <sup>2</sup> ]		Technical standards characteristic value [N/mm <sup>2</sup> ]	
			$P_S = 50\%$ $m = 3$	$P_S = 95\%$ $m = 3$	Fracture mechanic $P_S = 97.7\%$ $R = 0.5$	Effective notch stress $r_{ref} = 1 \text{ mm}$ $R = 0.5$	EC 3 <sup>1)</sup>   IIW <sup>2)</sup>	DNVGL-RP-C203 <sup>3)</sup>
01	20 mm	20.94	123.02	100.97	99	103	90	90
02	40 mm	33.07	116.68	95.46	92	102	82	84
-	60 mm	60.02	-	-	88	87	76	77
-	80 mm	60.02	-	-	90	88	71	77

<sup>1)</sup>  $k_s = (25 \text{ mm}/t)^{0.2}$

<sup>2)</sup>  $t > 25 \text{ mm}$ :  $f(t) = (25 \text{ mm}/t)^{0.2} \mid L/t > 2: t_{eff} = t \mid L/t \leq 2: t_{eff} = \max(0.5 \cdot L; t)$

<sup>3)</sup>  $t > 25 \text{ mm}$ :  $(25 \text{ mm}/t_{eff})^{0.2}$  with  $t_{eff} = \min((14 \text{ mm} + 0.66 \cdot L); T)$

With the knowledge of the weld seam geometry of butt-welded joints, a smaller reduction of the FAT-class was found for joints with plate thicknesses of  $t = 60$  mm and  $t = 80$  mm when evaluated with the two concepts. This is caused by lower secondary bending moment due to the linear misalignment  $e = 1.92$  mm for larger plate thicknesses  $t$ .

For plate thicknesses larger  $t > 25$  mm, a thickness reduction factor for butt-welded joints is used in the technical standards. A summary of reduced FAT-classes according to different technical standards can be found in Table 13. The reduction factor of the EC3 only consider the plate thickness  $t$ . In the IIW-Recommendations and in the DNVGL-RP-C203, the weld bead width  $L \triangleq b$  also influences this reduction factor. By using these different formulations on butt-welded joints with a plate thickness between  $t = 25$  mm and  $t = 80$  mm, the FAT-class decrease from 90 to 71 N/mm<sup>2</sup> for the EC3 and IIW-Recommendations and for the DNVGL-RP-C203 to 77 N/mm<sup>2</sup>. The numerical based fatigue strength analysis showed no indication of a reduction of this magnitude. This suggests a more benign plate thickness influence. The scope in the DVS-Technical Code 0905 [18] of the effective notch stress concept is limited to plate thicknesses  $t \leq 50$  mm. For this reason, the analysis carried out for plate thicknesses  $t = 60$  mm and  $t = 80$  mm are not covered by these recommendations. Nevertheless, the two calculation methods showed comparable results, and an applicability of the effective notch stress concept to larger plate thicknesses  $t$  seems to be given. The used calculations methods based on the consideration of the weld seam geometry and so the geometrical notch effects at the failure location. Next to this, the metallurgical notch effect and the residual stresses also influence the thickness reduction factor. In addition, for larger plate thicknesses, the number of internal defects increases with increasing seam volume due to multilayer technology. A general statement on the thickness reduction factor and the area of application of the effective notch stress concept seems only possible to a limited extent at the present time and should be further validated by tests.

## 6 Summary and outlook

In this paper, results from fatigue tests on butt-welded specimens made of different plate thicknesses  $t$  were presented. These butt welds were made by the submerged arc welding process which leads to weld seams with higher weld seam quality. Based on the fatigue tests carried out, a higher fatigue strength of butt-welded joints was found. Butt-welded joints can be classified in FAT-class 100 ( $m = 3$ ) if this manufacturing process is used. This requires compliance with the limit values for imperfections of the weld geometry acc. to ISO 5817 quality level B [3].

The tested specimens showed scattering at one stress level due to different geometrical irregularities. Nevertheless, a

safe FAT-class could be determined. In addition to these tests, investigations were carried out on large components. The results were within the scatter range of the small-scaled specimens and confirm the slope parameter  $m = 3$  of the S–N curves. Numerical simulations were also performed to find this increasing fatigue strength in the approaches as well. It could be shown a good compliance between the results from the fatigue tests and the FAT-classes determined by the effective notch stress and the fracture mechanic approach. Moreover, the fatigue resistance of larger plate thicknesses in a tower section was part of this study. The used weld imperfections were taken from a 3D scan of a weld seam geometry of a tower section. Both approaches result in comparable fatigue resistances and show a lower thickness reduction effect. This can be justified in terms of stress mechanics by the decay of the influence imperfections and is in contradiction with the specifications from the technical standards. These uniformly formulate a greater thickness reduction factor starting from a plate thickness of  $t = 25$  mm.

From the analyses, the following statements could be made about the influence of weld imperfections. Both, the weld overfill  $h$  and the weld toe angle  $\alpha$  affect this value without any interaction to the plate thickness  $t$ . The linear misalignment  $e$  and the plate thickness  $t$  are directly linked to each other and so the FAT value. A greater influence on this value is to be expected for smaller plate thicknesses  $t$ . In this analysis, the metallurgical notch effect and residual stresses were not considered. Caused by missing test results for butt-welded joints with larger plate thicknesses, a final assessment is not possible. Therefore, the authors believe that further research is needed on the structural detail of the butt-welded joint. The advantage of the crack propagation approach in comparison to other local or global approaches is the consideration of the crack length  $a$  as a parameter in the calculation. This can be used for non-destructive testing from the point of view of predicting the remaining service life or inspection intervals. Under the aspect of the re-evaluation of the FAT-class for submerged arc butt-welded joints, the service lifetimes of existing wind turbines can be extended. This is of economic interest in the context of an extension of the service lifetime after expiry of the approval period.

**Acknowledgements** The presented results from fatigue tests on butt-welded joints were largely worked out as part of a joint development project with ENERCON GmbH and NORDEX SE at Fraunhofer IGP and the University of Applied Science in Wismar. Special thanks go to ENERCON GmbH and NORDEX SE for providing the test results that made this article possible.

**Funding** Open Access funding enabled and organized by Projekt DEAL.

## Declarations

**Competing interests** The authors declare no competing interests.

**Open Access** This article is licensed under a Creative Commons Attribution 4.0 International License, which permits use, sharing, adaptation, distribution and reproduction in any medium or format, as long as you give appropriate credit to the original author(s) and the source, provide a link to the Creative Commons licence, and indicate if changes were made. The images or other third party material in this article are included in the article's Creative Commons licence, unless indicated otherwise in a credit line to the material. If material is not included in the article's Creative Commons licence and your intended use is not permitted by statutory regulation or exceeds the permitted use, you will need to obtain permission directly from the copyright holder. To view a copy of this licence, visit <http://creativecommons.org/licenses/by/4.0/>.

## References

- German Federal Ministry for Economic Affairs and Climate Action (2022) Informationsportal Erneuerbare Energien - Windenergie auf See - Ziele (Information Portal Renewable Energy - Wind Energy at Sea - Goals). <https://www.erneuerbare-energien.de/EE/Navigation/DE/Technologien/Windenergie-auf-See/Ziele/ziele.html>. Accessed 11 Mar 2022
- Glienke R, Kalkowsky F, Hobbacher AF et al. (2022) Bewertung der Ermüdungsfestigkeit von Rundnähten in Türmen von Windenergieanlagen – Ein Vergleich von experimentellen Untersuchungen und numerisch gestützter Nachweisführung auf Basis örtlicher Konzepte. DVS Congress (DVS-Berichte Band 382):678–702
- DIN EN ISO 5817:2023-07 (2023) Welding - fusion-welded joints in steel, nickel, titanium and their alloys (beam welding excluded) - Quality levels for imperfections (ISO 5817:2023); German version EN ISO 5817:2023
- Drebenstedt K, Kuhlmann U, Bartsch H et al. (2021) Neubewertung des Kerbfallkatalogs nach DIN EN 1993-1-9 (Re-evaluation of the detail categories according to DIN EN 1993-1-9). Stahlbau-Kalender 2021: Brücken; Neue Eurocode-Generation:367–434. <https://doi.org/10.1002/9783433610503.ch6>
- prEN 1993-1-9:2023 (2023) Eurocode 3: Design of steel structures - Part 1-9: Fatigue; German and English version prEN 1993-1-9:2023
- Feldmann M, Ummenhofer T, Kuhlmann U (2019) Neubewertung und Erweiterung des Kerbfallkatalogs nach Eurocode 3 für eine zukunftsfähige Auslegung hochbeanspruchter Stahlkonstruktionen. DAST Forschungsbericht 4/2019
- DIN EN 1993-1-9:2010-12 (2010) Eurocode 3: Design of steel structures - Part 1-9: Fatigue; German version EN 1993-1-9:2005 + AC:2009
- Hobbacher AF (2016) Recommendations for fatigue design of welded joints and components - second edition - IIW Document-2259-15. Springer Verlag, Wilhelmshaven
- Maschinenbau F (2020) FKM-guideline - analytical strength assessment, 7th edn. VDMA Verlag GmbH, Frankfurt am Main
- Gurney TR (1991) The fatigue strength of transverse fillet welded joints. Abington Publishing, Cambridge
- DNVGL-RP-C203 (2019) Fatigue design of offshore steel structures (Edition 2019-09 - Amended 2021-09)
- BS 7608+A1:2014-03-31 (2014) Guide to fatigue design and assessment of steel products
- DIN EN 13001-3-1:2019-03 (2019) Cranes - general design - part 3-1: limit states and proof of competence of steel structure; German version EN 13001-3-1:2012+A2:2018
- DIN EN ISO 6947:2020-02 (2020) Welding and allied processes - Welding positions (ISO 6947:2019); German version EN ISO 6947:2019
- IEC 61400-6:2020 (2020) Wind energy generation systems - part 6: tower and foundation design requirements
- DIN 18088-3:2019-01 (2019) Tragstrukturen für Windenergieanlagen und Plattformen - Teil 3: Stahlbauten (Structures for wind turbines and platforms - Part 3: Steel structures)
- Radaj D, Sonsino CM (2000) Ermüdungsfestigkeit von Schweißverbindungen nach lokalen Konzepten (Fatigue assessment of welded joints by local approaches). DVS-Fachbücher, Band 142, Düsseldorf
- DVS-Technical Code 0905:2021-05 (2021) Industrielle Anwendung des Kerbspannungskonzeptes für den Ermüdungsfestigkeitsnachweis von Schweißverbindungen (Industrial application of the notch stress concept for the fatigue strength verification of welded joints)
- Neuber H (1968) Über die Berücksichtigung der Spannungskonzentration bei Festigkeitsberechnungen (About the consideration of stress concentration in strength calculations). Konstruktion 20(7):245–251
- Radaj D (1985) Gestaltung und Berechnung von Schweißkonstruktionen – Ermüdungsfestigkeit (Design and calculation of welded structures - Fatigue strength). Fachbuchreihe Schweißtechnik
- Hobbacher AF (2005) Sicheres Bemessen nach den aktualisierten IIW-Empfehlungen zur Schwingfestigkeit (Safe design according to the updated IIW recommendations on fatigue strength). Festigkeit gefügter Bauteile - DVS Bericht 236:1–11
- Sonsino CM, Kaßner M (2005) Übersicht über Konzepte zur schwingfesten Bemessung von Schweißverbindungen (Overview of concepts for fatigue-resistant design of welded joints). Festigkeit gefügter Bauteile - DVS-Bericht 236:12–23
- Sonsino CM, Kaßner M, Fricke W (2009) Stand von Bemessungskonzepten zur schwingfesten Auslegung von Schweißverbindungen (State of the art of design concepts for fatigue-resistant design of welded joints). Festigkeit geschweißter Bauteile - DVS-Bericht 256:1–25
- BS 7910:2019 (2019) Guide to methods for assessing the acceptability of flaws in metallic structures
- API RP 579-1 / ASME FFS-1 (2021) Fitness-For-Service
- Maschinenbau F (2018) FKM-guideline - fracture mechanics proof of strength for engineering components, 4th edn. VDMA Verlag GmbH, Frankfurt am Main
- Sanz G (1980) Essai de mise au point d'une méthode quantitative de choix des qualités d'aciers vis-à-vis du risque de rupture fragile. La Revue de Métallurgie 77(7):621–642
- DIN EN 1993-1-10:2010-12 (2010) Eurocode 3: Design of steel structures - Part 1-10: Material toughness and through-thickness properties; German version EN 1993-1-10:2005 + AC:2009
- Hobbacher AF (2010) New developments at the recent update of the IIW recommendations for fatigue of welded joints and components. Steel Construction 3(4):231–242
- Berge S (1984) Effect of plate thickness in design of welded structures. Proc. Offshore Technology Conference, OTC Paper 4829, Houston
- DIN EN 1090-2:2018-09 (2018) Execution of steel structures and aluminium structures - part 2: technical requirements for steel structures; German version EN 1090-2:2018
- ISO/TR 14345:2012-06 (2012) Fatigue - Fatigue testing of welded components - Guidance
- DVS Technical Code 2403:2020-10 (2020) Empfehlungen für die Durchführung, Auswertung und Dokumentation von Schwingfestigkeitsuntersuchungen an Schweißverbindungen metallischer



- Werkstoffe (Recommendations for the performance, evaluation and documentation of fatigue tests on welded joints of metallic materials)
34. DIN EN ISO 9692-2:1999-09 (1999) Welding and allied processes - Joint preparation - Part 2: Submerged arc welding of steels (ISO 9692-2:1998, includes Corrigendum AC:1999); German version EN ISO 9692-2:1998 + AC:1999
  35. DIN EN 10025-2:2019-10 (2019) Hot rolled products of structural steels - Part 2: Technical delivery conditions for non-alloy structural steels; German version EN 10025-2:2019
  36. DIN EN ISO 6520-1:2007-11 (2007) Welding and allied processes - classification of geometric imperfections in metallic materials - part 1: fusion welding (ISO 6520-1:2007); Trilingual version EN ISO 6520-1:200
  37. ECCS - European Convention for Constructional Steelwork (2018) Background information on fatigue design rules -statistical evaluation (2nd edition): Technical Committee 6 Fatigue and Fracture No 140
  38. Jonsson B, Dobmann G, Hobbacher AF et al (2016) IIW guidelines on weld quality in relationship to fatigue strength. Springer, Paris, France. <https://doi.org/10.1007/978-3-319-19198-0>
  39. Glienke R, Kalkowsky F, Hobbacher AF et al. (2023) Evaluation of the fatigue resistance of butt welds in steel towers of wind turbines by fatigue tests and numerical based design with local approaches. 33rd International Ocean and Polar Engineering Conference (ISOPE), Ottawa, Canada

**Publisher's Note** Springer Nature remains neutral with regard to jurisdictional claims in published maps and institutional affiliations.